CENTRO DE INVESTIGACIONES
EN ÓPTICA, A.C.

POLARIZATION EFFECTS GENERATED THROUGH THE SCATTERING OF LIGHT BY METALLIC CYLINDERS

DOCTORADO EN CIENCIAS (ÓPTICA)

ADVISOR: DR. RAFAEL ESPINOSA LUNA

STUDENT: M. en C. IZCOATL SAUCEDO OROZCO

Febrero de 2017
León, Guanajuato, México

Abstract

In this work, the effects of the interaction between a thin metallic cylinder and a polarized optical field on the generation of both, unconventional and conventional polarization states are presented. In the first study, two different kinds of cylinders under conical incidence were analyzed: the first one was covered by a thin film of silver, which was done with the objective of improving the quality of the scattered light and reducing the possible effects of the scattering on the results in relationship with roughness on the surface; the second one was a nickel cylinder (an electric guitar string) chosen with the intention of proving that the method of generation is capable of giving good results without a well-defined surface and with a different diameter. The interactions of the lineal horizontal and vertical polarization states with the cylinders were measured around 360º, using a conical geometry of illumination, yielding azimuthal and radial polarization states as a resultant. The study of the scattered light after the cylinder leads to the application of the cylinder as a generator of unconventional polarization.

For the second study case, the cylinder was placed in the same system but with a different geometric configuration, under a plane geometry of incidence. The nickel cylinder was studied through the complete set of the six basic spatially homogeneous polarization states; the results obtained from the interaction between the cylinder and the polarization states show that the cylinder can be used as a wave retarder plate resolved angularly. The polarimetric analysis of this phenomenon provides new and original information and increases possible applications of the cylinder not only as a generator of unconventional states, but also as a wave retarder plate.

Resumen

En este trabajo se presentan los efectos de la interacción entre un cilindro metálico delgado y un campo óptico polarizado en la generación de estados de polarizaciones no convencionales y convencionales. En el primer estudio se analizan dos tipos diferentes de cilindros bajo incidencia cónica, el primero estaba cubierto por una delgada capa de plata, con el objetivo de mejorar la calidad de la luz dispersada y la reducción de los posibles efectos en los resultados relacionados con la rugosidad en la superficie. El segundo fue un cilindro de níquel (cuerda de guitarra eléctrica) elegido con la intención de probar que el método de generación es capaz de dar buenos resultados sin una superficie bien definida y con un diámetro diferente. La interacción de los estados lineales de polarización horizontal y vertical con los cilindros se midió alrededor de 360º, bajo una geometría de iluminación cónica, dando como resultado los estados de polarización radial y azimutal. El estudio de la luz dispersada después del cilindro conduce a la aplicación del cilindro como un generador de polarización no convencional.

Para el segundo caso de estudio, el cilindro de níquel fue colocado en el mismo sistema pero con una configuración geométrica diferente, en este caso una geometría de iluminación plana. El cilindro de níquel fue estudiado por el conjunto completo de los seis estados básicos de polarización espacialmente homogéneos; los resultados de la interacción entre ellos muestran que el cilindro puede ser utilizado como una placa retardadora de onda resuelta angularmente. El análisis polarimétrico de este fenómeno genera información nueva y original, lo que incrementa las posibles aplicaciones de los cilindros no sólo como generadores de estados no convencionales sino también como un retardador de onda resuelto angularmente.

Dedication

This work is dedicated to my family, especially to my parents Bruno and Araceli and my brothers Huitzilihuitl and Bruno, who have been there for me all the time. Thank you for all your guidance, time and advise; this would not have been accomplished without your support.

Acknowledgements

First of all, I would like to acknowledge the financial support from “Consejo Nacional de Ciencia y Tecnología (CONACyT),” whose grants made possible the research work leading to the Doctoral Degree (No. de becario 253212); I also thank CIO, which was part of my professional formation. This thesis work can only be presented as a result of that support.

I wish to thank to Dr. Rafael Espinosa Luna for giving me the opportunity to be part of his research projects. His scientific knowledge and experience in the field of optics have been a source of understanding and learning for me in the last six years. I owe him many thanks for his patience and unconditional support in my formation as a future researcher.

Abbreviations

LCOS	Liquid Crystal on Silicon
SLM	Spatial Light Modulator
CV	Cylindrical Beams
HG_{mn}	Hermite-Gauss solution
H_m	Hermite Polynomials
LG_{pl}	Laguerre-Gauss solution
VPSF	Vector Point Spread Function
LC	Nematic Liquid Crystal Cells
EOT	Extraordinary Optical Transmission
1-D	One Dimensional
PSG	Polarization Stage Generator
PSA	Polarization Stage Analyzer
LCVR	Crystal Variable Retarder
ARS	Angle Resolved Scattering System

Contents

Chapter 1

1.1 Introduction.

One of the fundamental properties of light is its vectorial and mathematical representation, the vectorial distribution along the optical axis which gives sense and direction to the optical field. Polarization plays an important role in the optical description of a medium and the vectorial definition of a source; the interactions between the light and matter can be easily described using polarization, and this kind of studies has been published in many research journals related to the field, where the development of new forms of polarization is in the interest of new research work [1-5].

The polarization theory is able to represent all the possible vectorial forms along of electromagnetic wave trajectory at any point. Saying that, polarization can be understood as an electromagnetic wave that has a direction of propagation where the interaction with the environment changes its features, but is always defined in some spatial distribution that might be homogeneous or non-homogeneous.

The problem to solve is how to explain the changes generated by the interaction of light with non-homogeneous materials when these have an internal structure, asymmetrical or symmetrical shapes, and a rough surface which jointly could constitute a multilayer system or a birefringent materials system. Incidence at arbitrary angles presents another variable to solve in the solutions of the representative equations of the system and the resultant polarized output beam. All of this makes it harder to understand and interpret an electromagnetic wave that is interacting with the environment through which the optical field is traveling. In the forms in which light can be found in nature, reflection and scattering are the primary generators of totally and partially polarized light. Many books and papers have been written on the various states of polarization in nature, not only on how to detect them, but also on the ways to define them.

The classic representation of polarization is based on a homogenous spatial distribution in the direction of propagation of the optical field at a given space or time coordinates. Unconventional polarization has a non-homogenous spatial distribution of the vectorial fields in the wave front of propagation of the optical field. This means that it is possible to find different combinations of classical polarizations in the same wave front. The search for new forms of response between the incident polarized light and the geometrical nature of the samples under study gives new answers that generate the need for different kinds of polarizations to better understand the interactions and possible applications in real problems.

There is a growing interest in this research area since radial and azimuthal polarizations have been applied to solve problems related in many optical areas. In optical trapping and optical tweezers, where some particles are considered difficult to trap, the strong axial moment of a highly focused radially polarized beam provides a large gradient force that helps in the solution of this problem [3, 4]. New effects and phenomena have been observed for optical fields with such unconventional polarization states; likewise, there are industrial applications where radial and azimuthal polarization states have an important role in the improvement production processes, such as in laser cutting and micro-drilling in steel [5].

This work presents two important results related with the generation of exotic states of polarization using a thin metallic cylinder under either conical or flat incidence geometry, respectively [6]. The use of the conical geometry of illumination allows the possibility of obtaining two kinds of unconventional polarization states, or spatially non-homogeneous polarization modes, from the light scattered by the thin metallic cylinder: azimuthal and radial. On the other hand, the light scattered by the thin metallic cylinder under a flat geometry of incidence has shown that the cylinder can be used as an angularly resolved wave-retarder [7]. As a result of our research, a new method to generate radial and azimuthal polarization was developed; furthermore, the experimental setup we used was modified and gave as a result new applications for the scattering of the light by the thin cylinder [6 and 7]. Recently, the research works related with the area of generation of unconventional polarizations have been developing different devices that are able to obtain the same results through different mechanisms; these new devices are dependent on the application of the resulting states of polarization [8 and 9].

One of our main interests was the generation of unconventional polarization using LCOS-SLM (Liquid Crystal on Silicon-Spatial Light Modulator) devices, with the objective of learning about new forms of generation of exotic fields; the advantages of working with the SLM is that it is possible to generate any desired state of polarization based on the configuration loaded onto each liquid crystal display [8].

1.2 Thesis layout.

The present work relates the use of classical polarization in the generation of unconventional polarization. This thesis is organized according to the following sequence:

Chapter 2 contains a brief description of the polarization theory, starting from the solution of the wave equation and how it takes importance when the orthogonal components of the field are related to each other. The amplitude and the phase shift between the orthogonal components define the resulting state of polarization for the classical mathematical representation. The general forms of representation of any classical state in one equation that contains the necessary parameters to give us the correct mathematical form that describes a polarized field in some direction (such as could be equations, vectors, or images) depend on how the polarization state has been measured. There are different representations of a defined polarization state; in this thesis, we are going to work with the Stokes vector representation as a manner to describe a state of polarization in its conventional form, and also we are going to try to understand the unconventional forms in terms of the Stokes formalism.

In the same chapter, it will be shown how the equations for the unconventional polarization take different representations, such as the cylindrical beams and their mathematical expressions in the general case; in this part of the thesis, the basic theory is presented for an adequate understanding of the following chapters.

Chapter 3 gives an experimental explanation about how an unconventional polarization can be obtained through the interaction of classical polarization states and a thin metallic cylinder under a conical geometry of incidence. In the same chapter, the second important research result is presented, with the same cylinder, but under flat incidence geometry; these results show how the light scattered from the thin metallic cylinder has properties that allow considering it as an angularly resolved wave retarder. Chapter 4 presents and discusses the conclusions generated by the research work.

In Appendix A, we are going to find the corresponding programs developed in MatLab software for the presentation and analysis of the results presented in Chapter 3; the Stokes formalism was developed and programmed with the aim of representing the data loaded in a graph of Stokes intensities vs scattered angle around 360º. In Appendix B, we are going to find a similar representation of the Stokes vectors obtained around 360º from the scattered light by the metallic thin cylinder, but now, data are represented in the Poincaré sphere, where it is possible to observe that the resulting polarization has a specific behavior around the sphere surface. The optical paths presented in the spheres are the polarimetric results measured with the PSA (polarization sates analyzer). In Appendix C, we are going to describe the programs developed in MatLab software for the presentation and analysis of the results presented in Chapter 3, where the polarimetric behavior of the cylinder shows that the cylinder can change the phase at four different points for two polarization states. In Appendix D, we are going to present the entire results for the case of conical incident polarization, the Stokes and Poincaré graphs for the ±45º polarization sates, and the right and left hand circular polarization states, these for the nickel and silver-coated fiber cylinders. In Appendix E, we are going to find the images taken to the fiber covered by silver and the nickel string; these images were taken with a Multiphoton Microscope.

1.3 Contribution.

This work seeks to show that it is possible to generate unconventional polarization with the application of the classical theory of polarized light. The necessity for different kinds of generation of unconventional polarization makes these results very important in the vectorial fields area. Although there are several alternatives in the market that generate the same polarization states, generated by different means, nowadays there are manufacturers that already offer their products to laboratories. In our study, we found that our system has advantages above the already existing ones. The main contribution of this work is the possibility to generate unconventional polarization states with a simple method, using a thin metallic cylinder mounted on a polarimetric experimental setup; the results show that it is possible to generate radial and azimuthal polarization states. The simple system configuration makes it more interesting for new applications. Another interesting result was found in the same experimental setup, but changing the angle of incidence, with the cylinder behaving as an angularly resolved wave-retarder. These results open new paths to using the thin cylinder, using polarization of the light as the way to understand the interaction, and yielding a new states of polarization and phase shift of light, where the wavelength is not the main problem, nor the laser intensity, but just the correct choice of the cylinder in terms of its index of refraction, diameter, and roughness.

1.4 Journal papers.

1. Izcoatl Saucedo-Orozco, Guadalupe López-Morales, and R. Espinosa-Luna, Generation of unconventional polarization from light scattered by metallic cylinders under conical incidence, Optics Letters **39** (18), 5341-5344 (2014).
2. Izcoatl Saucedo-Orozco, Rafael Espinosa-Luna, Qiwen Zhan, Angularly-resolved variable wave-retarder using light scattering from a thin metallic cylinder, Optics Communications **352,** 135-139 (2015).

Chapter 2

Summary

In this chapter, we are going to discuss the theory elements that are involved in the results that were obtained in this thesis work, on the basis of the principles that defined a solution of the wave equation generated from the Maxwell relations where the polarization of the electromagnetic field takes importance. The orthogonal components of the wave field are used with the objective of defining the most general kinds of polarization states, and its specials cases are related with the combination of amplitude and phase shift between the components of the electromagnetic field. The mathematical representation of a polarization state that is based on the general equation of ellipse of polarization was just the beginning of the introduction of a powerful tool in the optical characterization field. The necessity to have a system capable of representing any polarization state in its mathematical representation gives sense to the Stokes vector formalism; the common way to represent any polarization state depends directly on how we measure these states. There is another kind of representation of a polarization state through a sphere, called the Poincaré sphere; this method is able to show how polarization varies along of the surface of a sphere, where homogenous polarizations are well defined. The introduction to the mathematical representation of the cylindrical vectorial beams (CV) is presented as a reference of what kinds of wave fields we are going to be using for this thesis work; in the development of this theory, we are going to describe several modes of propagation of unconventional polarization states. Then, we are going to discuss the two forms of generation of these polarization states with the objective of showing the importance of our contributions to this emerging research field.

2.1 Polarization of light.

Polarization of light is considered a very important topic in physical science, basically in optics and photonics applications; this theory was developed with the objective of giving a better understanding of the phenomenon that occurs between the interaction of light and matter. When light has a well-defined sense and direction for a given period, it is possible to think about polarization; the polarization or state of polarization is the most common feature of an electromagnetic wave. The polarization refers to the behaviour of the wave vectors that correspond to the field observed at a fixed point in space [10].

The electromagnetic wave is described through four vectors: **E** electrical field, **H** magnetic field, **D** electric displacement field, and **B** density of magnetic flux [11]. The mathematical representation of these vectors is a set of partial differential equations that constitute the mathematical foundation of classical optics, and are also applicable in different research areas where physical phenomena associated with any kind of propagation of electromagnetic wave is present, even though any external condition can change their main features. Different kinds of solutions of the Maxwell equations are able to explain any of these phenomena. In the optical case, the equations that describe the propagation of the light are solutions of the following partial differential equations, and in this case, the medium of propagation is in the vacuum, without charge density or electric currents.

The partial differential equations for the electric and magnetic fields in vacuum are:

$$\nabla^2\vec{E}-\frac{1}{c^2}\frac{\partial^2\vec{E}}{\partial t^2}=0, \qquad \nabla^2\vec{B}-\frac{1}{c^2}\frac{\partial^2\vec{B}}{\partial t^2}=0, \tag{2.1.1}$$

The last relationships were deduced using the Maxwell equations [11 and 12]; the electric and magnetic fields are vector waves that can be changing along the direction of propagation. The basic solution of each wave equation (2.1.1), considering that the electric and magnetic fields travel along the z direction, has the next representation:

$$\vec{E}(r,t)=\vec{E}_0\cos(wt-\vec{k}\cdot\vec{r}+\delta), \tag{2.1.2}$$

where $\vec{r}=x\hat{i}+y\hat{j}+z\hat{k}$ is the position vector, and the spatial variation is called phase $\varphi=\vec{k}\cdot\vec{r}+\delta$. The vectorial nature of the light is called polarization [12]; to know the state of polarization for a wave, it is necessary to know the behavior of the orthogonal components of the field, if the direction of propagation is z; the vectorial field is described through the following relationships.

$$E_x(z,t) = E_{0x} \cos(\tau(z,t) + \delta_x) \tag{2.1.3}$$

$$E_y(z,t) = E_{0y} \cos(\tau(z,t) + \delta_y), \tag{2.1.4}$$

where E_{0x} and E_{0y} are the amplitude, δ_x and δ_y are the phases of the orthogonal components of the field, and $\tau = wt - kz$ is called the propagator. The propagation of the last two equations (2.1.3 and 2.1.4) results in a vector equivalent to their interaction along of the propagation direction [12]

$$\frac{E_x(z,t)}{E_{0x}} = \cos(\tau)\cos(\delta_x) - \sin(\tau)\sin(\delta_x) \tag{2.1.5}$$

$$\frac{E_y(z,t)}{E_{0y}} = \cos(\tau)\cos(\delta_y) - \sin(\tau)\sin(\delta_y) \tag{2.1.6}$$

Polarization has its own terminology, depending on whether the measurement sensor is located facing the laser or the opposite way; Continuous descriptions are going to be present in these terms. In the last equations (2.1.5 and 2.1.6), we will change the subscripts: *x* and *y* by *p* and *s*, respectively. These last equations are multiplied by the functions $cos\ (\delta_{p,s})$ and $sin(\delta_{p,s})$ and related between them through additions, giving as a result the following equations [12].

$$\frac{E_{ox}(z,t)}{E_{ox}}\sin(\delta_y) - \frac{E_{oy}(z,t)}{E_{oy}}\sin(\delta_x) = \cos(\tau)\cos(\delta_x - \delta_x) \tag{2.1.7}$$

$$\frac{E_{ox}(z,t)}{E_{ox}}\cos(\delta_y) - \frac{E_{ox}(z,t)}{E_{ox}}\cos(\delta_x) = \sin(\tau)\sin(\delta_y - \delta_x) \tag{2.1.8}$$

These equations help to determinate the general equation of elliptic polarization [12], which represents a general polarization state of an electromagnetic wave. With these representations of polarization, it is possible to describe six basic types of polarization states in a wave field. The elliptic polarization state is the most general kind of a monochromatic wave field; for the deduction of the elliptic representation, the equations (2.1.7 and 2.1.8) need to be related with each other.

Equations 2.1.7 and 2.1.8 are squared and then summed. The result of this is the next equation [12].

$$\frac{E_x(z,t)^2}{E_{ox}{}^2}+\frac{E_y(z,t)^2}{E_{oy}{}^2}-2\frac{E_x(z,t)}{E_{ox}}\frac{E_y(z,t)}{E_{oy}}\cos(\Delta)=sin^2(\Delta) \qquad (2.1.9)$$

Equation (2.1.9) is called the general equation of the polarization ellipse [12]. With this representation, it is possible to describe the six classical states of polarization with the correct combination between the phase difference and the amplitudes of the general equation of the polarization ellipse. The polarization states defined by are: linear horizontal, linear vertical, linear to +45º, linear to -45º, circular right-hand and circular left-hand.

The phase difference is defined as $\Delta=\delta_X-\delta_Y$. It can take a set of values, of which the most important are: 0, ±π, ±π/2; this occurs when the trigonometric functions behave as maximums or minimums, depending on the values of the phase shift. Modifications in amplitude occur when the orthogonal components are canceled, or when the magnitudes of the amplitudes are the same.

For the first case, when Δ=0, the state of polarization generated is linear (p polarization), while if Δ=π, the polarization generated is linear vertical (s polarization); all of this occurs when one of the amplitudes takes the value of zero. In the generation of the linear states, the general form is defined by the changes in amplitude and phase shift between the orthogonal fields of the optical field. For the case when the amplitudes are equal and the phase difference that corresponds to *Δ=0* or π, it is possible to generate ±45^o linear polarizations.

In the case when the difference of phase that corresponds to *Δ=±π/2*, it is possible to generate states with an elliptical polarization if their amplitudes are different; otherwise, if the amplitudes are the same, the generated states are circular right- and left-hand polarization states. If *Δ=π/2*, the generated state is circular right-hand polarization, and for the case when *Δ=-π/2*, the generated state is circular left-hand polarization. In all the cases, the values of the amplitudes of the orthogonal fields are the same and the observer registers looking to the source.

The previous paragraphs describe the generation of states of polarization through the combination of the phase difference and the changes in the values of the amplitude. These are able to generate any state of polarization. In the next diagram, it is possible to observe all of the variations on the phase and amplitude described above.

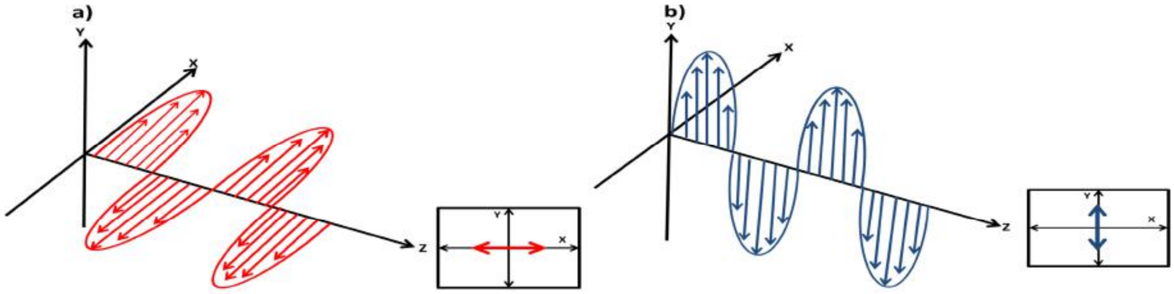

Fig. 2.1.1 a) Horizontal polarization representation (*p*), where Δ=0 and one component of the field corresponding to axis *y* is canceled. b) Vertical polarization representation (*s*), where Δ=0 and one component of the field corresponding to axis *x* is canceled.

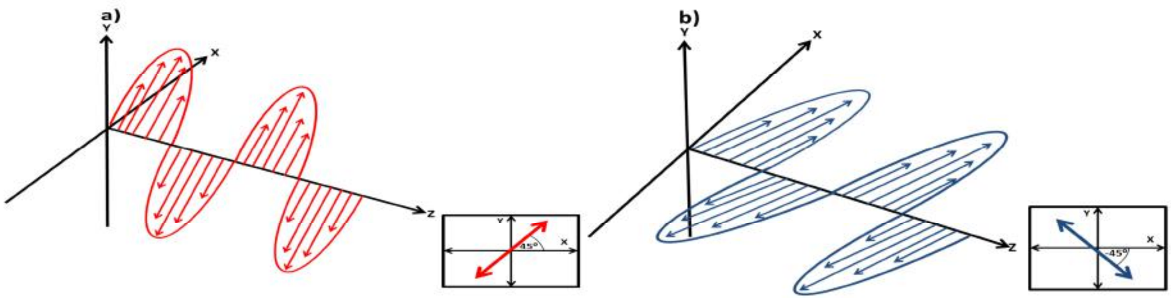

Fig. 2.1.2 a) +45º polarization representation (+), where Δ=0 and the components of the field are the same E_{0p}=E_{0s}. b) -45º polarization representation (-), where $\Delta=\pi$ and the components of the field are the same E_{0p}=E_{0s}.

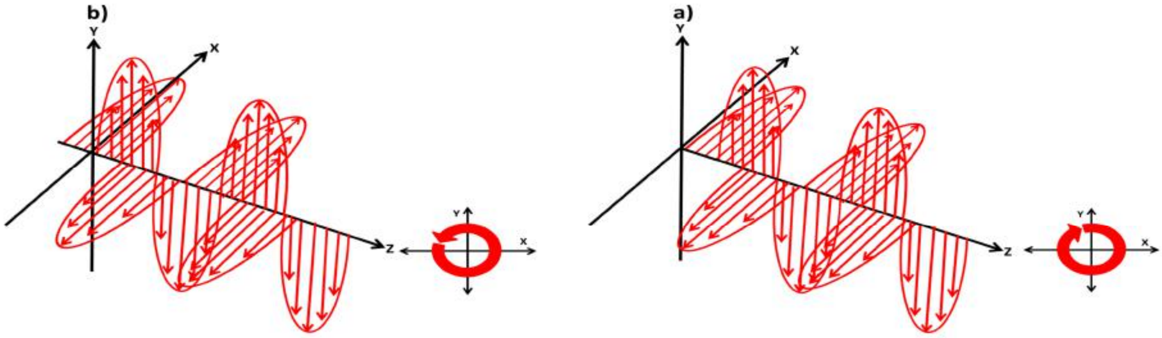

Fig. 2.1.3 (a) Circular right-hand polarization representation (r), where $\Delta=\pi/2$ and the components of the field are the same $E_{0p}=E_{0s}$. b) Circular left-hand circular polarization representation (*l*), where $\Delta=-\pi/2$ and the components of the field are the same $E_{0p}=E_{0s.}$

The last figures represent the cases in which the general equation of the ellipse of polarization takes different values depending on the parameters suggested in the relationship between amplitudes and phase shift difference.

It is important to describe the elliptical polarization state in terms of its fundamental features, which are ellipticity and azimuth. Because of these, the different polarization states can be described in function of such parameters. Although the determination of the resultant polarization state was based on the changes in amplitude and phase shift, the parameters to be considered are azimuth and ellipticity.

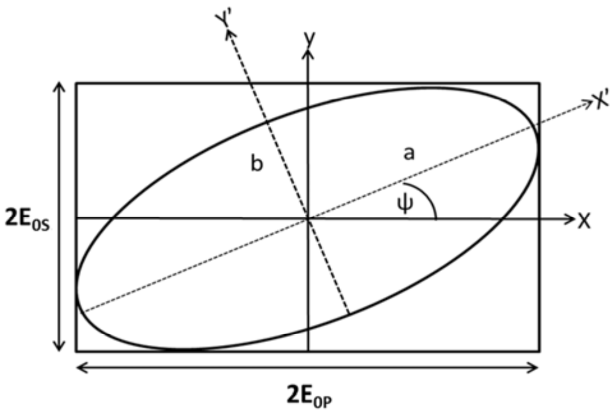

Fig. 2.1.4 Elliptical polarization representation; this figure was taken from [3].

In **Fig. 2.1.4**, it is possible to observe the representation of the elliptical polarization, where the principal features are the amplitudes (E_{0p}, E_{0s}), the azimuth angle (ψ) and the ellipticity (χ).

The rotation angle is defined by the next relationship [3],

$$\tan 2\psi = \frac{2E_{0p}E_{0s}}{E_{0p}^{\ 2} - E_{0s}^{\ 2}}\cos\Delta \qquad 0 \le \psi \le \pi \qquad (2.1.9)$$

The parameter of ellipticity is related with the ratios of the ellipse [1-3].

$$\tan\chi = \frac{\pm b}{a} \qquad -\frac{\pi}{4} \le \chi \le \frac{\pi}{4} \qquad (2.1.10)$$

2.2 Stokes Parameters.

In the search for new manners of representation of the states of polarization, Sir Gorge Gabriel Stokes, around 1842, proposed that the state of polarization could be represented in terms of observables; he described polarization in four parameters whose intensity can be measured directly [12]. This theory represents a polarization state on a vector whose dimentions are 4x1: the first parameter represents the total intensity of the electromagnetic field, while the rest of values of the vector are related to the behavior of the wave considering other kinds of polarizations which together define the state of polarization under study.

In the last section, the general equation of the ellipse of polarization was discussed; this helps to the generalization of a polarization state. The complete definition of any polarization state is not possible because azimuth and ellipticity are not directly measurable. With the correct combination of amplitudes and phase shift, it has been demonstrated that the general equation can be the basis for new kinds of polarizations at an instantaneous point. In order to figure this out, it is necessary to determine a time average of the electromagnetic field under study; the development of this theory provides the opportunity to represent polarization states in the shape of a vector [13]. Equation (2.2.1) is the representation of a Stokes vector related with a polarization state.

$$S = \begin{pmatrix} S_0 \\ S_1 \\ S_2 \\ S_3 \end{pmatrix} \tag{2.2.1}$$

In the deduction of the Stokes parameters as a function of observables, it is necessary to make a time average in the general equation of the ellipse of polarization (2.1.9). The amplitude and the phases of the wave field change in time, and the average is represented by the next relationship,

$$\left\langle E_i(t)E_j(t)\right\rangle = \lim_{T\to\infty}\frac{1}{T}\int_0^T E_i(t)E_j(t)\;dt \qquad i,\, j = x,\, y\,, \tag{2.2.2}$$

where T is the complete averaged time.

Applying the equation of time average (2.2.2) to the general equation of elliptical polarization (2.1.9), for which it is necessary to multiply the equation (2.1.9) per $4E_{0x}{}^2E_{0y}{}^2$, the next relationship is obtained [12]:

$$4E_{0y}{}^2\left\langle E_x(t)^2\right\rangle + 4E_{0x}{}^2\left\langle E_y(t)^2\right\rangle - 8E_{0y}E_{0x}\left\langle E_x(t)E_y(t)\right\rangle\cos\Delta = (2E_{0y}E_{0x}\sin\Delta)^2 \tag{2.2.3}$$

$$\left\langle E_x(t)^2\right\rangle = \frac{1}{2}E_{0x}{}^2 \tag{2.2.4}$$

$$\left\langle E_y(t)^2\right\rangle = \frac{1}{2}E_{0y}{}^2 \tag{2.2.5}$$

$$\left\langle E_x(t)E_y(t)\right\rangle = 2E_{0x}E_{0y}\cos\Delta \tag{2.2.6}$$

With the substitutions of the last equations in (2.2.3), we get:

$$S_0^2 = S_1^2 + S_2^2 + S_3^2 \tag{2.2.7}$$

Values S_0, S_1, S_2, and S_3 are observables of the optical field. These elements are defined by the following equations (they were introduced by Stokes as a result of his theory).

$$S_0 = E_{0x}{}^2 + E_{0y}{}^2 \tag{2.2.8}$$

$$S_1 = E_{0x}{}^2 - E_{0y}{}^2 \tag{2.2.9}$$

$$S_2 = 2E_{0x}E_{0y}\cos\Delta \tag{2.2.10}$$

$$S_3 = 2E_{0x}E_{0y}\sin\Delta \tag{2.2.11}$$

The Stokes parameters represent any polarization state of an electromagnetic wave, for the case of total state of polarization it is necessary to prove the identity $S_0^2=S_1^2+S_2^2+S_3^2$. In the process of the analysis where the point of observation takes an important relevancy, the directions and orientations of the field are related directly with the point of observation or measurement of the polarization states.

The S_0 represents all the intensity of the incident light, S_1 represents the linear states of polarization, if the value of this is positive that means horizontal polarization; on the other hand, if the value of this parameter is negative, that means vertical polarization is obtained. S_2 represents the ± 45º of states of polarizations. If the value of this parameter is positive this means a +45º polarization states, for the case of negative value -45º of polarization state. S_3 represents the circular right- and left-hand polarization states, when the value is positive this means the circular right-hand polarization state, on the other hand the negative value means circular left-hand polarization state.

Another form to describe a wave filed is in polar representation, the Stokes parameters can be expressed in complex notation.

$$\begin{aligned} E_x(t) &= E_{0x}e^{i\delta x}e^{i\omega t} \\ E_y(t) &= E_{0y}e^{i\delta y}e^{i\omega t} \end{aligned} \tag{2.2.13}$$

The representation of the Stokes vector under this configuration is:

$$S = \begin{pmatrix} E_xE_x{}^* + E_yE_y{}^* \\ E_xE_x{}^* - E_yE_y{}^* \\ E_xE_y{}^* + E_yE_x{}^* \\ i\left(E_xE_y{}^* - E_yE_x{}^*\right) \end{pmatrix} \tag{2.2.14}$$

Where $i=\sqrt{-1}$ and * represents the complex conjugate. The main properties of the Stokes vector are related with the possibility of represent any state of polarization; the capability of being using the orthogonal components of the optical field gives sense to the next vectorial representation.

$$S=\begin{pmatrix} S_0 \\ S_1 \\ S_2 \\ S_3 \end{pmatrix}=\begin{pmatrix} E_{0x}{}^2+E_{0y}{}^2 \\ E_{0x}{}^2-E_{0y}{}^2 \\ 2E_{0x}E_{0y}\cos\Delta \\ 2E_{0x}E_{0y}\sin\Delta \end{pmatrix} \tag{2.2.15}$$

Using the previous definition of the Stokes vector, any polarized state can be represented, particularly the six basic polarization states mentioned previously. The Stokes vector that represents a horizontal linear polarization is (S_H), the Stokes vector that represents a vertical linear polarization is (S_V), the Stokes vector that represents a +45º linear polarization is (S_+), the Stokes vector that represents a -45º linear polarization is (S_-), the Stokes vector that represents a circular right-hand polarization is (S_R), and the Stokes vector that represents a circular left-hand polarization is (S_L). The Figs. 2.2.1 to 2.2.3 show the relation between the Stokes vector and the graphical form of the optical field.

$$S_H=I_0\begin{pmatrix} 1 \\ 1 \\ 0 \\ 0 \end{pmatrix}$$

$$S_V=I_0\begin{pmatrix} 1 \\ -1 \\ 0 \\ 0 \end{pmatrix}$$

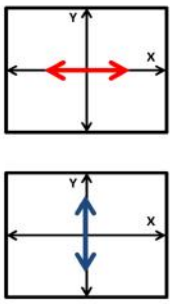

Fig. 2.2.1 Stokes vector and graphical representation of the linear polarization states, S_H horizontal polarization state, S_v vertical polarization state, where I_0 is the intensity and is normalized to the unity.

$$S_+ = I_0 \begin{pmatrix} 1 \\ 0 \\ 1 \\ 0 \end{pmatrix} \qquad S_- = I_0 \begin{pmatrix} 1 \\ 0 \\ -1 \\ 0 \end{pmatrix}$$

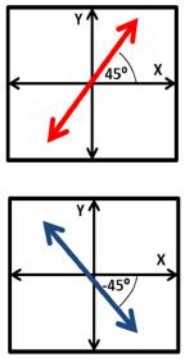

Fig. 2.2.2 Stokes vector and graphical representation of the linear polarization states, S_+ +45º polarization state, S_- -45º polarization state, where I_0 is the intensity and is normalized to the unity.

$$S_R = \begin{pmatrix} 1 \\ 0 \\ 0 \\ 1 \end{pmatrix} \qquad S_L = \begin{pmatrix} 1 \\ 0 \\ 0 \\ -1 \end{pmatrix}$$

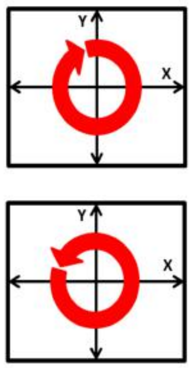

Fig. 2.2.3 Stokes vector and graphical representations of the circulars polarization states, S_R right-hand polarization state, S_L circular left-hand polarization state, where I_0 is the intensity and is normalized to the unity.

The Stokes vectors are related with the orientation (or azimuth ψ) and the ellipticity (χ) angles [12].

$$\begin{aligned} S_0 &= 1 \\ S_1 &= \cos(2\psi)\cos(2\chi) \\ S_2 &= \sin(2\psi)\cos(2\chi) \\ S_3 &= \sin(2\chi) \end{aligned} \qquad (2.2.16)$$

The angles are defined by the follow equations [4].

$$\psi = \frac{1}{2}\tan^{-1}\left(\frac{S_2}{S_1}\right) \quad 0 \leq \psi \leq \pi \tag{2.2.17}$$

$$\chi = \frac{1}{2}\tan^{-1}\left(\frac{S_3}{S_0}\right) \quad -\frac{\pi}{4} \leq \chi \leq \frac{\pi}{4} \tag{2.2.18}$$

The mathematical description of the Stokes vector has been deduced in the past paragraphs, but the next question comes from the necessity of measure the corresponding state from any source of light. The Stokes parameters can be measured using two polarized elements, a linear polarizer and a retarder wave plate both with the correct orientations.

The classical form to measure the Stokes parameters is performed by passing the optical field through two polarization elements; these elements can be a wave plate retarder and a linear polarizer. It is possible to use an unpolarized source or polarized, and the sensor can be any detector, but always taking into account that we are registering intensities. The retarder waveplate introduces a phase shift (α) between the orthogonal components of the optical field, this spatial delay is related with the fast axis of the retarder waveplate, the change in the phase can be controlled by different forms, in the most common case the fast axis of the retarder waveplate is clearly marked by the manufacturer. The most frequently retarder wave-plates used in the laboratories are: λ/2 and λ/4, the values of the phase shift between the orthogonal fields are π/2 and π/4, respectively. The linear polarizer transmits the component of the optical field that goes through its transmission axis; this axis can be oriented in any azimuthal direction (θ) [13]. The intensity that the detector measure has the mathematical representation [13]:

$$I(\theta,\alpha) = \frac{1}{2}\left[S_o + S_1\cos 2\theta + S_2\sin 2\theta\cos\alpha - S_3\sin 2\theta\sin\alpha\right]. \tag{2.2.19}$$

The Fig. 2.2.4 describes the experimental setup for the measurement of the Stokes vector from any source. The retarder waveplate and the linear polarizer are fitted in the setup with the objective to analyze six incident polarizations states. These polarized elements can be rotated for the complete analysis. The polarizer will have three specifics positions, when θ = 0, π/2, and π/2.

The retarder wave plate will have only two specific positions, when α = 0, and π/2.

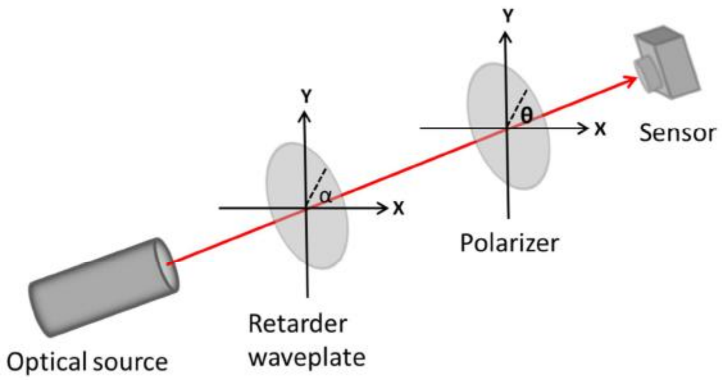

Fig. 2.2.4 Experimental setup developed for the classical measurement of the Stokes vector, the retarder waveplate and the polarizer work as analyzer for the six polarization states.

The mathematical representation of the resultant Stokes vector from the complete measurement has the following form, equation (2.2.20). These intensities are measured by the sensor showed in the Fig. 2.2.4. The intensities are described as in the equation (2.2.19).

$$S^{out}=\begin{pmatrix} S_0 \\ S_1 \\ S_2 \\ S_3 \end{pmatrix}=\begin{pmatrix} I(\theta,\alpha)+I(\theta,\alpha) \\ I(\theta,\alpha)-I(\theta,\alpha) \\ 2I(\theta,\alpha)-S_0 \\ S_0-2I(\theta,\alpha) \end{pmatrix}=\begin{pmatrix} I(0,0)+I\left(\frac{\pi}{2},0\right) \\ I(0,0)-I\left(\frac{\pi}{2},0\right) \\ 2I\left(\frac{\pi}{4},0\right)-S_0 \\ S_0-2I\left(\frac{\pi}{4},\frac{\pi}{2}\right) \end{pmatrix} \tag{2.2.20}$$

The applications for the Stokes vector are increasing in nowadays; the capability to determine and represent any possible polarization state makes this tool essential for the light behavior representation. The Stokes vector can be used as a form of measurement of the real time space variations polarization, where the results represent a polarization state at each location [14].

The last description of the Stokes vector was done in terms of intensities, but not only is this kind of form is possible to find them in the literature. The technique of imaging polarimetry has been increasing in the last couple of years, as a tool that is capable to represent a polarization state in images; this means a rectangular distribution of information that in many of the cases the matrices include information about polarimetric changes that were generated by different phenomena. Polarized light as a tool of analysis in the remote sensing where the spectral sensors tend to provide information about the vector nature of the optical field across the scene [15 and 16]. In the past section was discussed that the polarization can be generated by the diffraction produced in the interaction between the light and a surface with roughness, where the Stokes vector analysis is an important tool at the time to give an interpretation of the results that are showed as images [17]. In the nature, all type of waves can be associated a specific polarization state, even those that do not have a classical behavior, this means, they do not have the six defined polarization states as the linear and circulars [18], even though there are other forms of polarimetric analysis, the most useful and applied in this area of research is the Stokes vector.

The polarimetric analysis can be used as an important tool in the understanding of the vectorial nature of an electromagnetic wave, with its analytical mathematical representation in a vector or matrix, the polarization imaging has played important role in the biological studies. Biomedical polarimetry is still at a relative early stage of development, although this technique has an extensive loss of quality of polarization state by the tissue scattering under study [19- 21], even though these problems there are present in the real experimental applications, the polarimetric characterization of a biological sample has been applying for the noninvasive studies.

There are some metrics related with the Stokes vector and the Mueller matrix that help to understand some issues when the simple polarimetric analysis is not enough or when the changes induced by the sample have specific orientation in the resultant optical field. The Mueller matrix is rectangular representation of the polarimetric response of any system, this form to observe the medium helps to understand the possible mathematical representation of a polarized element, and then their possible simulation using any software [22 and 23]. In the general case, the Stokes parameters represent the most powerful tool and easily to measure for any polarized state, this simplicity gives the opportunity to the Stokes vector to be continued as an important tool when the polarization is the topic of interest. The development of this section was with the objective to present the necessary tools for the future presentation of the results where the Stokes theory helps in analysis of them.

2.3 Poincarè sphere.

The Poincaré sphere is an alternative representation of any total polarization state. The ellipse of polarization is another model of representation, but in this form it is not possible to describe partially polarized states for the definitions of ellipticity and azimuth. In order to solve the problem of determining the polarization of a beam after that has passed through some polarizing elements, the direct relation between the Stokes parameters, the orientation (azimuth), and ellipticity are the key to solve this problem. In this thesis work, the Poincaré sphere would be defined in function of the values of the Stokes vectors.

Around 1890 Henri Poincaré found that the ellipse of polarization can be represented in the complex plane with the projection of a sphere [12], in those days it was difficult to do calculations involving polarized light which could not be represented easily using the general elliptical representation, and even more complicated with the configurations where the use of polarized elements were included. The most relevant features of the Poincaré sphere are two: the first refers that is possible to represent any point on the surface of the sphere as a defined total polarization state, and that this state is described with three Stokes parameters (considering a normalization with respect to the total intensity is applied). As was discussed in the past sections, this kind of representation helps in to the understanding of the light as a vector and its polarimetric behavior in which it has a specific numerical structure, and it has a defined state of polarization that could be any of the conventional six polarization states before mentioned, these polarization states could be identified in the surface of the sphere as a defined point that has its three Stokes values. The second is related with the necessity to describe the behavior of optical polarizing elements. The **Fig. 2.3.1** represents the Poincaré sphere in Cartesian coordinates.

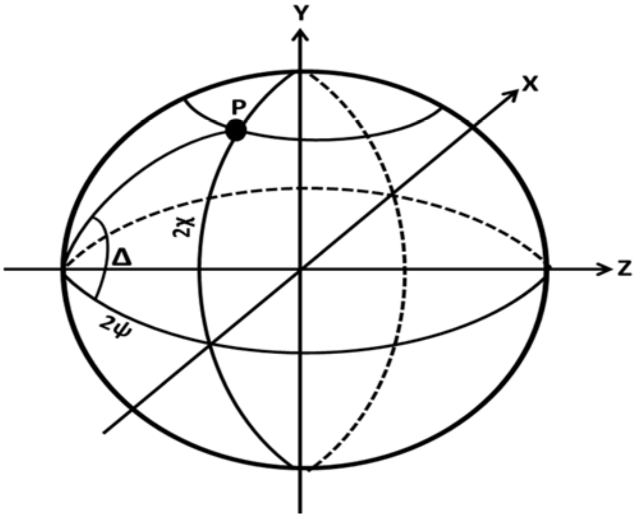

Fig. 2.3.1 Poincaré sphere in Cartesian coordinates, ψ and χ are the angles of azimuth and ellipticity. Any point in the surface can be represented in function of the past mentioned parameters and in the Stokes representation.

The Stokes parameters in a Poincaré sphere with radius equal to the unity in the intensity can be written in the similar form as the Eq. (2.2.16).

$$\begin{aligned} S_0 &= 1 \\ S_1 &= \cos(2\psi)\cos(2\chi) \\ S_2 &= \sin(2\psi)\cos(2\chi) \\ S_3 &= \sin(2\psi) \end{aligned} \qquad (2.3.1)$$

A point in the Poincaré sphere is represented by latitude angle 2χ and longitude angle 2ψ, where a polarization state is described by P(2χ,2ψ).

With the relations (2.3.1) it is possible to represent any polarization state in the Poincaré sphere, this in function of the coordinates (2ψ, 2χ) [12]. The horizontal polarization state is represented for the coordinates P (0^o, 0^o), vertical polarization state S (180^o, 0^o), linear polarization of +45º X (90^o, 0^o), linear polarization of -45º Y (270^o, 0^o), circular right-hand polarization state R (0^o,90^o) and circular left-hand polarization state L (0^o, -90^o).

The forms of representation of the polarization states are possible to represent in the Poincaré sphere with a radius equal to the unit (normalized). The following Figures show the points that represent the six classical polarization states in the surface of the sphere, it is important to point out that the axes of the sphere are the Stokes parameters, each point in the sphere has a Stokes vector defined.

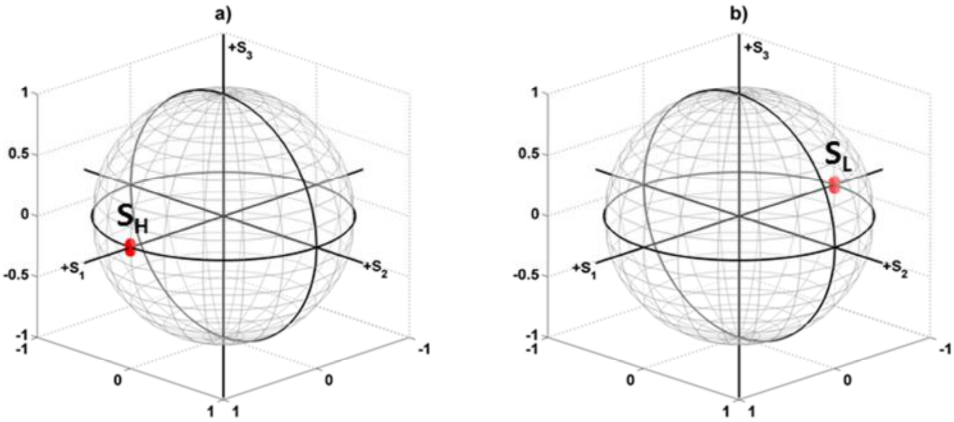

Fig. 2.3.2 The linear polarization states are possible to represent in the Poincaré sphere, each state has a specific position in the surface of the sphere. a) Horizontal polarization state, this state can be related with the Stokes vector S_H, but it is possible to relate in function of azimuth and ellipticity as in the **Fig. 2.3.1.** b) Vertical polarization state, this state can be related with the Stokes vector S_V, but it is possible to relate in function of azimuth and ellipticity as in the **Fig. 2.3.1.**

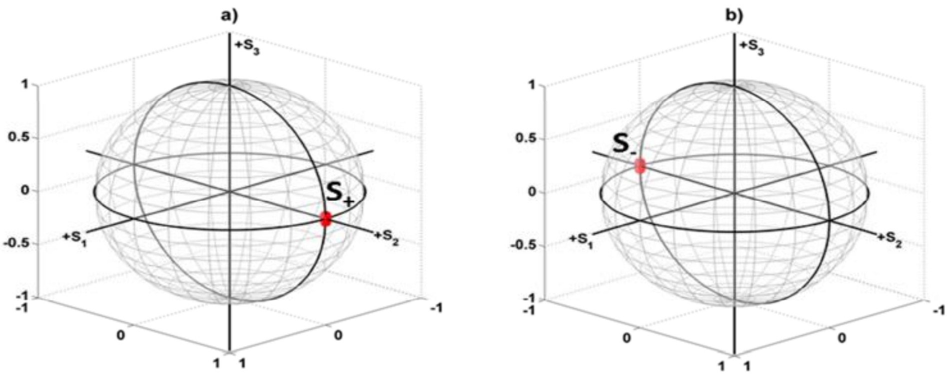

Fig. 2.3.3 The linear polarization states are possible to represent in the Poincaré sphere, each state has a specific position in the surface of the sphere. a) Linear + 45º polarization state, this state can be related with the Stokes vector S_+, but it is possible to relate in function of azimuth and ellipticity as in the **Fig. 2.3.1.** b) Linear -45º polarization state, this state can be related with the Stokes vector S_-, but it is possible to relate in function of azimuth and ellipticity as in the **Fig. 2.3.1.**

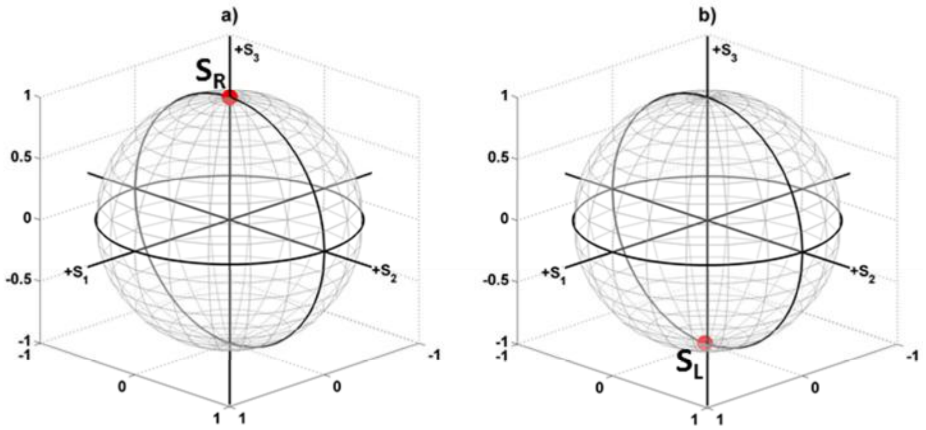

Fig. 2.3.4 The circular polarization states that are possible to represent in the Poincaré sphere, each state has a specific position in the surface of the sphere. a) Circular right-hand r polarization state, this state can be related with the Stokes vector S_R, but it is possible to relate in function of azimuth and ellipticity as in the **Fig. 2.3.1.** b) Circular left-hand l polarization state, this state can be related with the Stokes vector S_L, but it is possible to relate in function of azimuth and ellipticity as in the **Fig. 2.3.1.**

One of the principal applications of the Poincaré sphere is the possibility to represent the resultant polarization state of an optical beam after its transmission through some polarized elements. For the six classical polarizations states, the sphere had been defined by the poles or around the meridians.

The Fig. 2.3.5 shows the Poincaré sphere where is included the behavior of a retarder wave plate (in his Mueller matrix representation) which is rotated through 0º to 360º, the incident beam has a +45º polarization state, this beam passes through the retarder wave plate at the same time that the plate is rotating, the resultant polarization in the sphere is presented where the changes around the rotation defined the resultant polarization state and the same form a Stokes vector representative to those states. Nowadays the utility of this kind of polarimetric representation has taken a big importance since its first development and application on this research area, by the same reason that the classical polarization has moved to different research topics, the Poincaré sphere did the same actualization. Now with a big challenge that is the capability to represent all the unconventional polarization states, one of the principals objectives of this thesis.

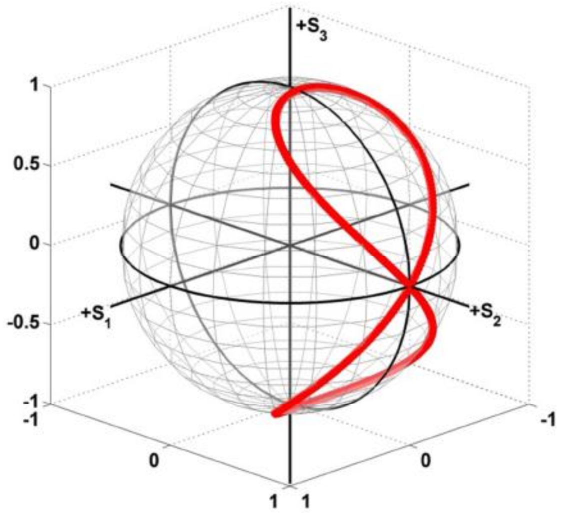

Fig. 2.3.5 The Poincaré sphere that represents the output beam of an optical setup composed by a wave retarder with a specific rotation and a linear polarizer oriented to +45º. Around the path described in the 360º, is possible to see the behavior of the beam, passing through the poles where the circular left- and right-hand polarization states are defined.

New forms of representation of the Poincaré sphere have been developed, for the cases where the classical form cannot be capable of represent a polarizations state, new spheres have been developing for the cases of exotic polarization states. The new Poincaré sphere is constructed by extending the Jones vector basis to the general vector with the continuously changeable ellipticity (spin angular momentum) and the higher dimensional orbital angular momentum [24].

The changes induced in an optical wave field can be represented by its paths described around the surface of the Poincaré sphere. There is a method based on analysis of torsion and curvature of three-dimensional segments, three-dimensional curves segments are defined by series of points representing the polarization state. These changes in the direction are reflected by the field and described in the Poincaré sphere [25]. The Mueller matrix can be the most representative form of how the medium responds under the linear interaction with polarized light. The Mueller matrix representation is combined with the Poincaré sphere with the objective to give the better understanding of a phenomenon where the Mueller matrix of the medium is completely described by a set of three associated ellipsoids whose geometrical and topological properties are characteristic of the resultant matrix [26].

It is well known about the different forms of propagation of the electromagnetic field, following this line the next question is related with the necessity to know the type of resultant polarization on these fields. But before answer this question, the main point is to know how those fields were generated, and give them the correct interpretation or representation. The dynamic propagation of the optical field generated through an optical vortex has been recently applied in the unconventional polarization states generation area. Optical beams with rotationally polarization symmetry are incorporated into the Poincaré sphere representation [27]. The development of this section was done with the objective to present the necessary tools for the future presentation of the results where the Poincaré sphere helps in analysis of them.

2.4 Cylindrical vector beams.

Cylindrical vector (CV) beams are considered a special class of optical vector fields as an axially symmetric beam solution to the full vector electromagnetic wave equation [28]. The previous sections were employed to describe that optical fields are vectorial beam solutions of the Maxwell equations, but in this case the equations have an axial symmetry in both amplitude and phase. In this section we will introduce the difference between two concepts: the spatial homogeneous polarization state or conventional polarization and the spatial non-homogeneous or unconventional polarization state. The first was discussed in the past sections in its general features, the classical or homogeneous polarization states are understood as vectorial fields with a specific spatial distribution along the optical axis, and this means that in a certain spatial point of the field we will find a polarizations state well defined, then in another point we will have the same direction on the vectorial fields that represent the same polarizations state, this along of the propagation medium. The second represent the contrary case, when the vector field has not a combination of wave vectors in the same spatial distribution; this means that it is possible to find wave vectors with different directions or combinations of polarization states at the same point.

In the past years the researchers found more interesting properties of the CV beams, this increased the scientific production in this research area, with potential applications in imaging, particle trapping, sensing, etc. The applications of the CV beams have drawn increasing interest in the vectorial wave research area, researchers continue to come up new concepts for unconventionally polarized beams and are developing techniques to generate and characterized them [29]. In the development of this section we will mention some of these interesting research journals that had reported some of the most relevant research results, our interest will be focused in the study of two unconventional polarization states: azimuthal and radial.

The mathematical description of the CV beams is developed the in same form as the other wave solutions that are obtained by solving the scalar Helmholtz equation.

$$\left(\nabla^2 + k^2\right)E = 0 \tag{2.4.1}$$

In Cartesians coordinates the paraxial solution for the electric field takes the next form:

$$E(x,y,z,t) = u(x,y,z)e^{i(kz-wt)}. \tag{2.4.2}$$

Appling the following approximations to the last equation, the slowly varying approximation are obtained [28]:

$$\begin{gathered} \frac{\partial^2 u}{\partial z^2} << k^2 u \\ \frac{\partial^2 u}{\partial z^2} << k\frac{\partial u}{\partial z} \end{gathered} \tag{2.4.3}$$

By separation of variables of x and y can be obtained the Hermite-Gauss solution HG_{mn}, these solutions have the following representation [28]:

$$u(x,y,z) = E_0 H_m\left(\sqrt{2}\,\frac{x}{w(z)}\right)H_n\left(\sqrt{2}\,\frac{y}{w(z)}\right)\frac{w_0}{w(z)}\exp\left[-i\phi_{mn}(z)\right]\exp\left[\frac{ikr^2}{2q(z)}\right] \tag{2.4.4}$$

Where the H_m denotes the Hermite polynomials and it satisfy the next differential equation [28]:

$$\frac{d^2 H_m}{dx^2} - 2x\frac{dH_m}{dx} + 2mH_m = 0 \tag{2.4.5}$$

Where the $w(z)$ is the beam size, w_0 is the beam size at the beam waist, $z_0=\pi w_0^2/\lambda$ is the Rayleigh range, $q(z)=z-iz_0$ is the complex beam parameter, and $\phi_{mn}(z)=(m+n+1)\tan^{-1}(z/z_0)$ is the Gouy phase shift. If the conditions of m=n=0 are applied to the last equation reduces to the fundamental representation of a Gaussian beam [28].

For a paraxial solution in cylindrical coordinates, the solution takes the following representation [28]

$$E(r,\phi,z,t) = u(r,\phi,z)e^{i(kz-wt)}. \tag{2.4.6}$$

Substituting the last equation (2.4.6) in to the scalar Helmholtz equation (2.4.1), and applying the slowly varying approximation, the following equation is obtained [28]:

$$\frac{1}{r}\frac{\partial}{\partial r}\left(r\frac{\partial u}{\partial r}\right)+\frac{1}{r^2}\frac{\partial^2 u}{\partial \phi^2}+2ik\frac{\partial u}{\partial z}=0 \tag{2.4.7}$$

From the last equation, the Laguerre-Gauss solution LG_{pl} modes can be deduced applying separation of variables of *r* and ϕ, the previous step results [28]:

$$u(r,\phi,z)=E_0\left(\sqrt{2}\frac{r}{w}\right)^l L_p^l\left(2\frac{r^2}{w(z)}\right)\frac{w_0}{w(z)}\exp\left[-i\phi_{pl}(z)\right]\exp\left[\frac{ikr^2}{2q(z)}\right]\exp(il\phi). \tag{2.4.8}$$

Where $L_p^l\,(x)$ represent the Laguerre polynomials and satisfies the next differential equation [28].

$$x\frac{d^2L_p^l}{dx^2}-(l-1-x)\frac{dL_p^l}{dx}+pL_p^l=0 \tag{2.4.9}$$

Another type of solution from the equation (2.4.7) that obeys the rotational symmetry is the following relation [28]:

$$u(r,z)=E_0\left(\frac{w_0}{w(z)}\right)\exp(-i\phi(z))\exp\left(i\frac{kr^2}{2q(z)}\right)J_0\left(\frac{\beta r}{1+\frac{iz}{z_0}}\right)\exp\left(-\frac{\beta^2\frac{z}{2k}}{1+\frac{iz}{z_0}}\right) \tag{2.4.10}$$

In the last relation it is possible to observe the zeroth-order Bessel function of the first kind, β represents a scalar parameter. The solutions before discussed are valid in the paraxial field approximation and they focus in the Helmholtz equation which corresponds to conventional polarizations or scalar fields where the trajectory of oscillation does not depend of the point of view inside of the transversal section [28].

The vector solution with its direction aligned in the azimuthal orientation takes the next equation form [28]:

$$E(r,z) = U(r,z)\exp[i(kz - wt)]\vec{e}_{\phi} \tag{2.4.11}$$

Where the last equation is a solution of the following relation: $\nabla\times\nabla\times\vec{E} - k^2\vec{E} = 0$. Where the relation *U(r, z)* satisfies the next differential equation [28]:

$$\frac{1}{r}\frac{\partial}{\partial r}\left(r\frac{\partial U}{\partial r}\right) + \frac{U}{r^2} + 2ik\frac{\partial U}{\partial z} = 0 \tag{2.4.12}$$

One solution of the equation (2.4.12) corresponds to an *azimuthally polarized* vector Bessel-Gauss beam solution (2.4.13), where the *u(r, z)* is a fundamental Gaussian solution [28].

$$U(r,z) = E_0 J_1\left(\frac{\beta r}{1+\frac{iz}{z_0}}\right)\exp\left(-\frac{i\beta^2\frac{z}{2k}}{1+\frac{iz}{z_0}}\right)u(r,z) \tag{2.4.13}$$

The other solution of the equation (2.4.12) corresponds to transverse magnetic solution. Where H_0 is magnetic field amplitude, the $\vec{h}_{\phi}$ is the unit vector in the azimuthal direction. This azimuthal magnetic field solution represents the *radial polarization* (2.4.14) of an electric field [28].

$$H(r,z) = -H_0 J_1\left(\frac{\beta r}{1+\frac{iz}{z_0}}\right)\exp\left(-\frac{i\beta^2\frac{z}{2k}}{1+\frac{iz}{z_0}}\right)u(r,z)\exp[i(kz - wt)]\vec{h}_{\phi} \tag{2.4.14}$$

The generation and propagation of the spatial distributions of the instantaneous electric field vector for several linearly polarized Hermite-Gauss and Laguerre-Gauss modes and the CV beams modes are illustrated in the **Fig. 2.4.1.** All the modes have different features that make them useful in many research areas, in our case; the main point is to find a new form to generate that kind of polarization states.

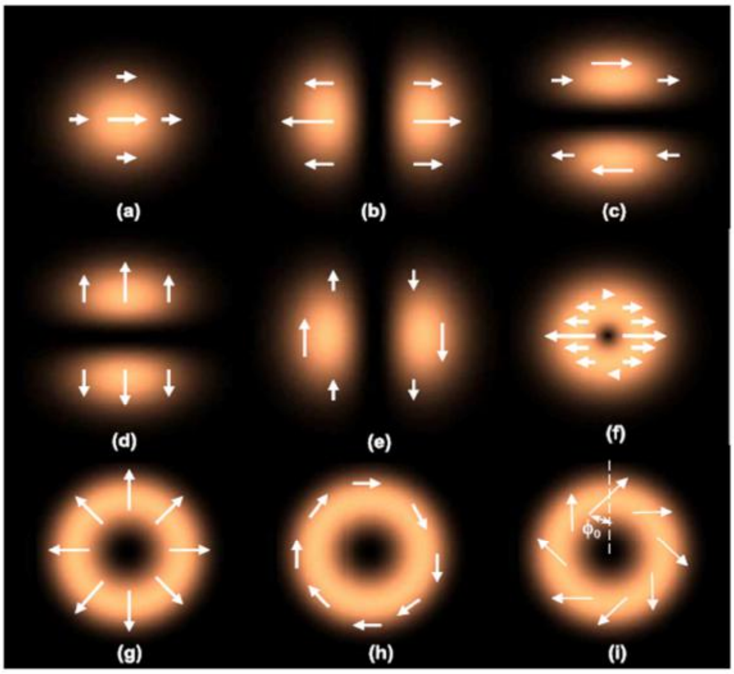

Fig. 2.4.1 Spatial distributions for different modes of propagation of the instantaneous electromagnetic wave field, homogenous and unconventional polarizations states represented as CV beams. (a) x-polarized fundamental Gaussian mode; (b) x-polarized H_{G01} mode; (c) x-polarized H_{G01} mode; (d) y-polarized H_{G01} mode; (e) y-polarized H_{G10} mode; (f) x-polarized L_{G01} mode; (g) radially polarized mode; (h) azimuthally polarized mode; (i) generalized CV beams as a linear superposition of (g) and (h); this image was taken from [28].

Since the invention of the laser, the research and the new knowledge about the uses and applications of this device, this has provided new forms to solve some issues that until his invention were not possible to solve. The laser plays a fundamental role in the optics and photonics research areas, where the most common uses concerns to the physics, chemistry, information technology, material processing, industrial cutting, precision measurement, equipment manufacturing, among many other application areas. All of these applications were studied since the beginnings of this invention, but not all of its potential was exploited until that the interest increased with the propagation of the laser light (how the photons are traveling throughout its path).

The research on optical fields is focused in the homogeneous cases: linear fields with elliptic polarization state, field with circular polarization state, that of behavior of the optical field are called scalar optical fields.

The development of new forms of generation of the scalar optical field was the principal point in this research area; their applications related with structured fields gave results to some present problems. Thereby, the interaction between the matter and these kinds of polarization states solved some of the existents optical phenomena, although not all of the systems gave the desired result. The necessity of answers where the scalar optical fields are useless gave the opportunity to the new forms of polarization states. In this section, we focus on two particular descriptions of unconventional polarizations. These states refer the case when the treatment of the vector optical field takes importance in its distribution of amplitude and phase. The possible applications, where the form of generation define the possibilities of success in the results, therefore, we are going to explain in what cases the resultant polarization states are considerate as unconventional polarization, and theirs applications of a form to study the medium.

There are two different forms to generate unconventional polarization states [30]; one of them is called active method. This technic involves the use of a laser as the generator of the vector optical fields with unconventional polarizations. It is well known that the output beam from a laser can be modified from the laser cavity, the variations in the mode of propagation of the output beam are related with the medium in which the internal beam has interaction. The devices with internal cavity have an axial birefringent component or axial dichroic component to provide mode discrimination against the fundamental mode [30]. For the generation of radial polarization state it was designed and fabricated a Brewster angle element that consist of a convex and concave conical prism, where was deposited a dielectric multilayer for the election of the output polarization beam, all of these were done in the cavity of a Nd:YAG laser [31]. The generation of a radial polarized laser beam using a birefringent material in a crystal laser, an improvement of the power efficiency and a reduction of the cavity size, these improvements support the selective oscillation with radial polarization using at the birefringence of a laser crystal [32].

On the other hand, the passive method for the generation of unconventional polarization is used in the most of the cases. This technique converts those known as spatially homogeneous polarization states (lineal and circular polarization states) into unconventional polarized optical fields, which can be described as CV beams. The most of the experimental setups are done in a free space, this means that, in contrast with the past described method, now the generation of unconventional polarizations states is done outside of the laser cavity or the illuminating source employed.

It is important to point up that in this case for the generation of unconventional polarization states is necessary to use as a input beam the spatially homogeneous polarization states, which means that the variations of the resultant field depends directly of the method designed in the experimental setup. The most common equipment that the researchers use for the generation of these states are the optical devices as birefringence elements, dichroic systems, retarder plates, polarization gratings, and spatial light modulators, among many others.

Another very popular and useful form of generation of unconventional polarization states are the spatial liquid modulators (SLM) in reflection or transmission. The SLM offers the possibility of generate almost any complex field distribution which means that in the nowadays research journals have a lot of information and techniques with variations of different focus but the same idea of generation of these kind of fields, in many forms and for spatial applications. The use of two SLMs to control the vector point spread function (VPSF) of a microscopic objective, where this makes possible to control the relative phase of the electric field in the objective pupil in order to measure the resultant polarization in the focus point [33].

The generation of vectorial optical fields using the SLMs presents the possibility to control the orthogonal components of the incident electric field, where the SLM is used as a variable and addressable retarder. Based on two reflective SLMs it was designed and fitted an experimental setup capable of controlling all the parameters of the spatial distributions of an optical field, including the phase, amplitude, and polarization on a pixel by pixel basis [34]. The reflective liquid crystal device has a specific resolution which varies depending of the quality and the manufacturer, and the phase shift can be controlled pixel by pixel too. Due to the birefringent nature of the SLM, the system responds to the horizontal component, meaning that the reflected beam is going to carry the waveform loaded in the SLM while the vertical component is going to be reflected with no affectation [34]. The control of the polarization with a nematic liquid crystal cells (LC) just with an adjustment in the voltage applied in the section of the LC, the amount of rotation with respect to each axis from three LC gets as a resultant output beam with specific polarization state, represented in the Poincaré sphere [35].

The capability to modify the incident beam using a SLM and the necessity of more complex vector optical fields makes its use essential in this research area. The use of optical vortex to modify an incident beam with the objective to have as output a beam with a spatial non-homogeneous distribution makes this method another important technique to generate unconventional polarization states with many applications nowadays [34-36]. The combination of optical vortexes with positive and negative topological charges gives as a result an azimuthal two-beam interference effect, this idea of multiple vortex beams with different topological charges creates a pattern with interference along the azimuthal coordinate, and this can be useful in optical trapping and construction of diffraction gratings [36].

The generation and application of the unconventional polarization states are included in different research areas, for the many problems to solve. These states are useful in almost all the optics sub-areas. For example, in the optical fiber where the mode of propagation of the electric field inside of the fiber takes a significant importance for a big amount of applications. Not only the capability of maintaining or generate the state of polarization along all the fiber but also the possibility to change the output beam polarization as we want [37]. Choosing the right parameters in an optical fiber, the generation of radial polarization states can be possible just based on the mode selection inside of the optical fiber rather than the laser cavity. The multi-mode optical fiber accepts several angular modes [38].

The combination of different optical techniques with the objective to generate as a resultant an output field with unconventional polarization has rapidly been increasing its applications in several areas of research. The descriptions of new form of generate exotic polarization states (called like this for their complexity) with the combination of a 4-F system, spatial liquid modulator (SLM) and an interferometric arrangement, where any desired beam can be generated [39]. The utility of these special cases of CV beams like the azimuthal and the radial, where they have already developed several applications about them, the recent research journals have reported some applications using the angular momentum that carry these kinds of polarization states [40 and 41]. Typical examples are the optical trapping, optical tweezers, high-resolution microscopy, lasers, biological studies, among many others, the unconventional polarization always will be present [42-49]. The development of this section was with the objective to present the necessary tools for the future presentation of the results where the cylindrical vector beams play a relevant role.

Chapter 3

Summary
In Chapter 3, we are going to talk about the experimental setup proposed and its results. In the past sections was mentioned that the principal objective of this thesis work was the generation of unconventional polarization states as a result of the interaction between polarized light and a metallic cylinder. In the first section we are going to describe the proposal form of generation for that kind of states, where the interaction between a thin metallic cylinder and a polarized beam under conical incidence gives a new method of generation. which works with a spatially homogenous polarized light as incident beam, for the generation of azimuthal and radial states, the incident beams are have horizontal and vertical polarizations, respectively. The light scattered through the interaction between the incident beam and the cylinder was recollected by a polarization states analyzer, and the representation of this data was represented using the Stokes vectors around 360º. In the second section of this Chapter we are going to show other results that we found in the interaction between the thin cylinder and the four remaining basic homogeneous polarization states, where the results are presented also in the formalism of Stokes vector and the Poincaré sphere. These results show that the thin cylinder can be used as a wave retarder resolved angularly, and in the Poincaré sphere they were described as paths around the surface of the sphere, from 0º to 360º. At the end of each section we are going to discuss some of the conclusions generated by the two experimental setups employed here.

3.1 Generation of unconventional polarization from light scattered by a metallic cylinder under conical incidence.

This section includes the results obtained in the first published article [6]. In this section, we are going to discuss a new form of generation of unconventional polarization states, in particular azimuthal and radial; at the same time we are going to mention some of the existent methods of generation with the objective to compare the proposed method with the others.

In the past sections were described briefly how the passive generation of unconventional polarization works, the main idea is that all of the equipment necessary in a free space condition; this means that it is possible to fit an experimental setup in an optical table without any problem; in a comparison with the active methods, where the mode of conversion is performed inside of the cavity of a laser, for example, there are methods where the selection of radial and azimuthal polarization states is done through birefringence induced in a simple laser resonator [42,43].

In this section of the thesis, we are going to present the first part of our experimental results; this work consists of a simple experimental method capable of generate unconventional polarized states from the scattered light generated by the interaction of a polarized light and a thin cylinder.

The results show a new way to generate radial and azimuthal polarization states; this opens the possibility to use that kind of polarizations in a broad range of applications like industrial, remote sensing, biological characterization, optical tweezers, laser cut, super resolution, antennas, among many others.

The capacity of changing the field components around the focus point applying radial and azimuthal polarization states makes these optical waves are being studied and applied in many areas; One example of these states occurs when they are focused by high-NA objective lenses for the better understand of the nonlinear signal generation in biological tissue [44]. The use of trapping forces with polarized light is presented like the best option for particles manipulation research, in the cases, when the scale of the systems under study are small, like particles, proteins, nanosystems, nanostructured systems among others. Optical tweezers have become a common tool in the optical trapping and moving micro objects, where the use of unconventional polarization states has been increasing by its components of the optical field, in the case of radially polarized light, which contributes to the improvement of the gradient force [45-48].

Since the discovery of extraordinary optical transmission (EOT) and its combination with unconventional polarization states for new ways and applications in the vectorial optical fields research area [49], this phenomenon is related with a subwavelength structures and can be explained through the excitation of electromagnetic resonance modes in some structures [50]. The radial and azimuthal polarization states present a polarization contrast when they are used as highly focused beams in coaxial apertures. The structures in nanoscale play an important role in the EOT setups, like the nanoantenna that generates more efficient connection of the incident photon energy [51 and 52].

Our principal interest in this thesis work is to generate unconventional polarized light using existing tools in laboratory, finding the best and easy way to generate that kind of states. The scattering of the light by a one dimensional surface (1-D, surface whose profile changes only along one direction) can generate changes in the incident polarization state; the 1-D surface is defined with respect to a reference system, and in this case the Cartesian coordinates are going to describe the orientation of the surface. In the most common cases, the study of 1-D surfaces only make use of scattered light in the plane of incidence, and only through horizontal and vertical polarization states, in other cases the full polarization analysis is presented [53-56].

The **Fig. 3.1.1** shows the scattering geometry for the study of a 1-D surface, under a conical geometry of incidence [54]. However, in most of the studies reported, the scattering of light by one-dimensional randomly rough surfaces has been realized under plane configurations of illumination some time ago [57–62].

In this thesis work, we are going to use a thin metallic cylinder as a 1-D surface, looking for the polarimetric response around 360º; the scattered light by one-dimensional surfaces under conical or off-axis geometry of incidence, these generate a cone of scattered light, this cone is formed in the same plane of the surface of the optical table. If we are using a one-dimensional surface, the axis of this cone of light is located along the generators (or grooves) of the surface [54], for the case when we are using a thin metallic cylinder, the axis is going to be located in its axis. This can be observed in the **Fig. 3.1.1**.

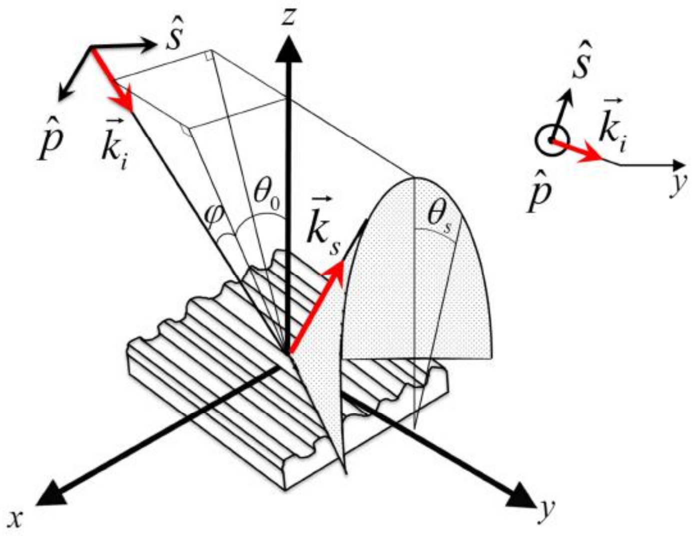

Fig. 3.1.1 Schematic diagram of the scattering geometry. The scheme shows the two unitary vectors, p and s, defining the polarization with respect to the plane defined by k_i (incident vector field) and the y axis, this Figure was taken from [54]. K_s represents the scattered vector field, θ_s represents the scattered angle,

In the **Fig. 3.1.1** if the flat geometry is changed to a conical geometry of incidence ($\varphi \neq 0$), the first experimental work reported that the s-scattered polarization is maintained always perpendicular to the cone's surface, whereas the π-scattered polarization is always tangential to the surface of the cone [54]. This means, the generation of the unconventional polarized states azimuthal and radial by one-dimensional surfaces was reported some time ago [54], but it was never reported by using thin metallic cylinders instead of 1-D surfaces, as we are going to show it in the following paragraphs.

Nowadays there are many investigation fields for the generation of unconventional polarization states (radial and azimuthal); those methods are based in different theories depending of their application. One important technique in this research area is the use of an s-waveplate; this plate is able to convert lineal polarization to radial or azimuthal polarization [63]. The generation of unconventional polarization states using an s-wave plate against the Gaussian wave front distribution present interesting differences between each other, the advantages and disadvantages are related with the area of application [64 and 65]. Another interesting way to generate unconventional polarization states was mentioned in the past sections; this is related to the use of spatial liquid modulators (SLM), where with the combination of different optical techniques this modulators and the s-wave plate have become a useful tool in the vectorial optical field [66-72].

3.1.1 Theory.

The generation of unconventional polarization states using the passive method allows the use of retarders, polarizers, spatial liquid crystal modulators, interferometric arrangements, scattering surfaces, among others; all of this with the objective to generate non-homogeneous polarization states (in the majority of the cases radial and azimuthal polarization states).

Nowadays the generation of unconventional polarizations (azimuthal and radial particularly) with the use of s-wave plate has become increasingly popular in the research topics [64-72]. In this thesis work, we are going to present a new form of generation of unconventional polarization through the interaction between a thin cylinder and homogeneous polarization states [6].

We defined the 1-D surface as a rough system (surface, thin cylinder, diffraction grating, among others) with respect to a Cartesian coordinate system as a surface whose profile (z-axis) varies only along the x-axis and is constant along the y-axis. The scattering properties of 1-D rough metallic and dielectric surfaces have been extensively reported theoretically, numerically and experimentally, where the polarized light has been used as a tool of analysis. The Stoke vector, Poincaré sphere, and Mueller matrices have been used as mechanism to understand the polarimetric response of the system [73-83].

The study of cylinders with light has potential applications in the solution of many problems: radiative transfer, remote sensing, and diagnosis, among others. Metallic cylinders have been one of the main geometries studied [84-91]. Some authors have developed an optical technique for the automatic detection of surface defects on thin metallic cylinder (wire) that can be used in on-line systems for surface quality control; this technique is based on the intensity variations on the scattered cone generated when the wire is illuminated by a polarized beam at oblique incidence [92 and 93]. The existing methods do not put interest in the input polarized light because their experiments do not depend on the polarimetric response, leaving a big branch for our research about the application of different polarization states as input beams under conical incidence.

Another theory that helps with the representation of a polarization state is the Stokes vector, discussed in the previous sections, where a vectorial arrangement can be used as the mathematical representation of polarized light. In this thesis work, we are going to describe the states in function of Stokes vectors around a full circle of 360º; the advantage of this method is the capability of representing any case of polarization state. The generation of the six basic incident polarizations states was done through a lineal polarizer and a variable retarder wave-plate; we are going to discuss this mechanism in the following sections, and for the generation of radial and azimuthal polarization states were only necessary two polarization states. The rest of experimental results would be described in the Chapter 5, **Appendix D**.

In this thesis work, one of the main objective are related with the studies obtained in the diffraction of the light through the cylinders at an off-axis or conical diffraction geometry. These results can be interpreted under the unconventional polarization scope, as associated to radial and azimuthal polarizations.

3.1.2 Methods.

A simple method is proposed in this thesis, for the generation of unconventional polarization states as the radial and azimuthal kinds; an experimental setup capable of measure the scattered light generated by a metallic cylinder, illuminated at 632.8 nm, under a conical or off-axis geometry. A great advantage of the method presented here is related to its inherent possibility to generate these unconventional polarization states with no limit on the wavelength employed once the cylinder material and its thickness are selected appropriately, provided that the cylinder radius is greater than the illuminating wavelength [94 and 97]; this opens up the possibility for a broad range of applications, from surgery to industrial and even to remote sensing.

This study was applied in two different types of cylinders: the first, an optical fiber covered with a uniformly distributed aluminum thin film (deposited with an evaporation chamber) with diameter of 232 µm, and the second, a metallic thin cylinder of nickel (string for an electric guitar) with diameter of 254 µm. All of these diameters were measured with a Veeco/Bruker, Dektak 6M surface profiler. The thickness of the aluminum evaporated in the surface of the fiber was measured using the same procedure, first without the deposited film and after with the deposited film; the thickness of the film deposited was approximately 53µm (the optical fiber had a diameter of 125µm). The **Fig. 3.1.2** shows the experimental setup.

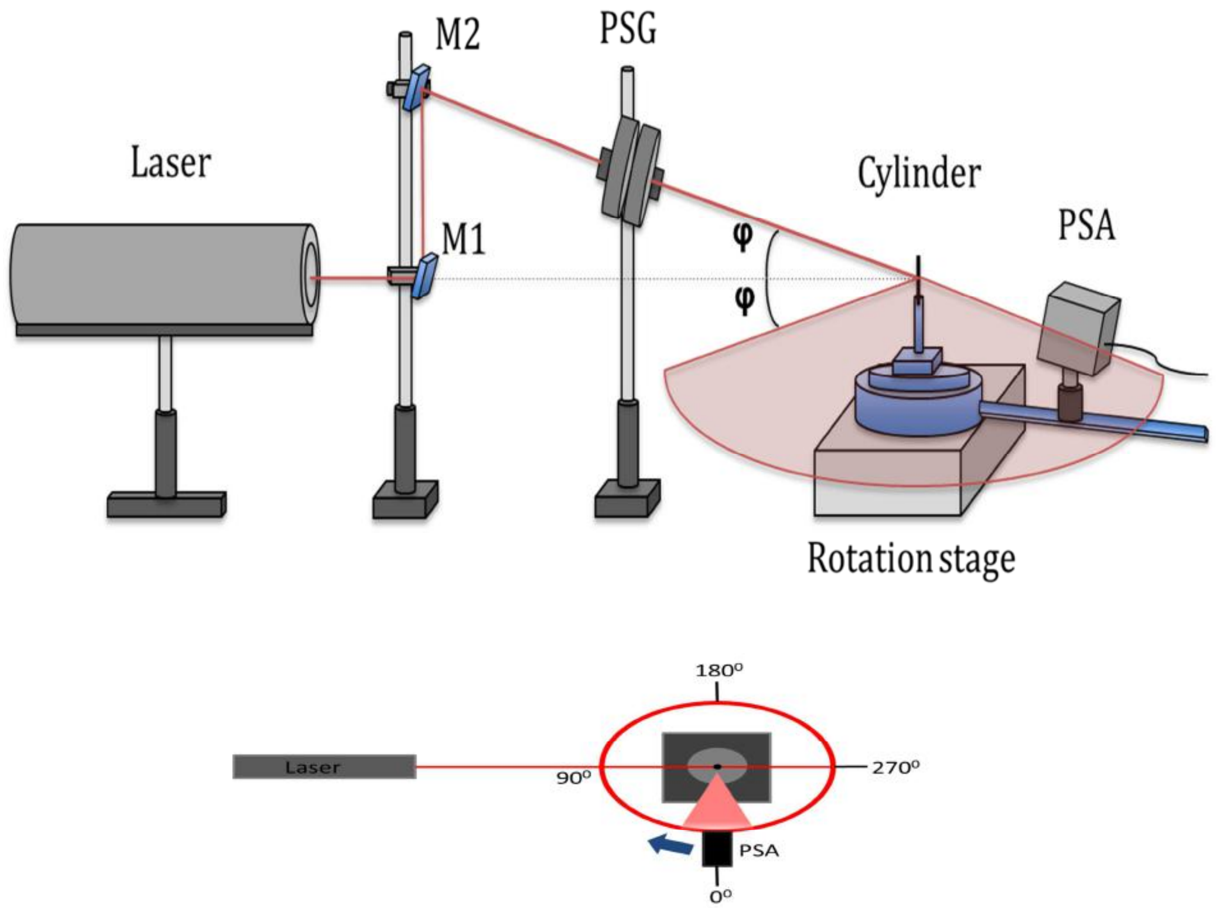

Fig. 3.1.2 Experimental setup employed for the measurement of the light scattered by the metallic cylinder under conical incidence, the lower describe the methodology of measurement of the vector parameters.

Within the experimental setup were used two mirrors (M1 and M2), a HeNe laser with a wavelength of 632 nm, a polarization stage generator (PSG), and a polarization stage analyzer (PSA). The size of the collimated beam was 2 mm of wide and it was send to the cylinder. The PSG consists of a combination of a linear polarizer of the Glan-Thompson type and a liquid crystal variable retarder (LCVR) with controller from Thorlabs, models LCC1111-A and LCC25, respectively [98 and 99]. Once the linear polarizer and the LCVR are mounted into motorized rotating mounts, they can be operated as a polarizing state generator (PSG) to generate any incident conventional polarization state.

The PSA is a commercially available head from Thorlabs, model PAX5710/VIS [100]; The measurement setup inside of this device consist of a combination of a retarder wave plate (with a retardance of $\lambda/4$) rotating with some frequency, then a lineal polarizer, and then a silicon sensor which measure the changes in the polarization generated by any sample. The PSA was placed on a rigid arm 40 cm from the cylinder; the cylinder was placed at the center of an automated rotation stage of an angle resolved scattering system (ARS). The angle φ corresponds to the conical angle, when the angle takes a null value corresponds to a flat or plane incidence geometry, i.e. Light beam strikes perpendicularly the cylinder. The diffraction pattern generated by the interaction of the light with the cylinder is located in the plane of the incident beam; this pattern describes a cone which contains all the information of the changes in the polarization state of the incident light.

The experimental setup has been calibrated with respect to the incident intensity associated with each parallel, p, or perpendicular, s, incident linear polarization state in the plane geometry, and it was also verified for the conical geometry (π-generated, π-detected and σ-generated, σ-detected), see Fig. 3.1.1); This means that, in the absence of any polarization sensitive effects in the optical medium placed between the PSG and the PSA (without any cylinder under study), any polarization state detected corresponds to the same polarization state generated.

The experimental data obtained were plotted as normalized scattered Stokes vectors versus the scattering angle (measured in degrees) for each of the two incident polarization states used herein. The intensity of each scattered Stokes parameter has been determined in one full turn, from 0º to 360º, where the data acquisition begins at 0º (**Figs. 3.1.1** and **3.1.2**). The beam is incident at an angle θ_0= 0º and a conical angle φ= 4.0º (**Fig. 3.1.2**). This means that the incident light is content along the line that defines 90º and 270º, as observed from the PSA on the arm of the scatterometer.

The Stokes parameter S_0 represents the total intensity, $S_1 > 0(< 0)$ is associated with the tendency to p-polarization (s-polarization), $S_2 > 0(< 0)$ indicates the tendency to linear +45 (−45) polarization, and $S_3 > 0(< 0)$ indicates the circular right-hand (left-hand) polarization sense. This interpretation can be verified in the past sections (Chapter 2) where it was described the vectorial representation of the polarized light.

The **Fig. 3.1.3** shows the light scattered angularly, represented by the four Stokes parameters, when a σ-polarization state (s-polarization state) is incident in the aluminum cylinder at $\theta_0 = 0^o$ and a conical angle φ (this polarization is reduced to the s-polarization state when the conical angle is zero).

Almost all the total energy is scattered uniformly as a negative S_1 Stokes parameter [$S_1(\theta_{scatt}) \approx -1$]. Using the terminology defined in **Fig. 3.1.1** for the conical geometry, the scattered light is highly associated with a σ-polarization state. A small intensity peak is present at 270º (the propagation direction of the incident beam, measured from the scatterometer arm) in the S_2 and S_3 scattered Stokes parameters, surely generated by the scattered waves at the Fraunhofer region.

Our experience has shown us that the presence of small S_2 and S_3 contributions can be reduced if a perfect alignment is reached and a small-roughness cylinder is used (we have employed a simple hand-made mount to hold the cylinder and a commercial electric guitar string).

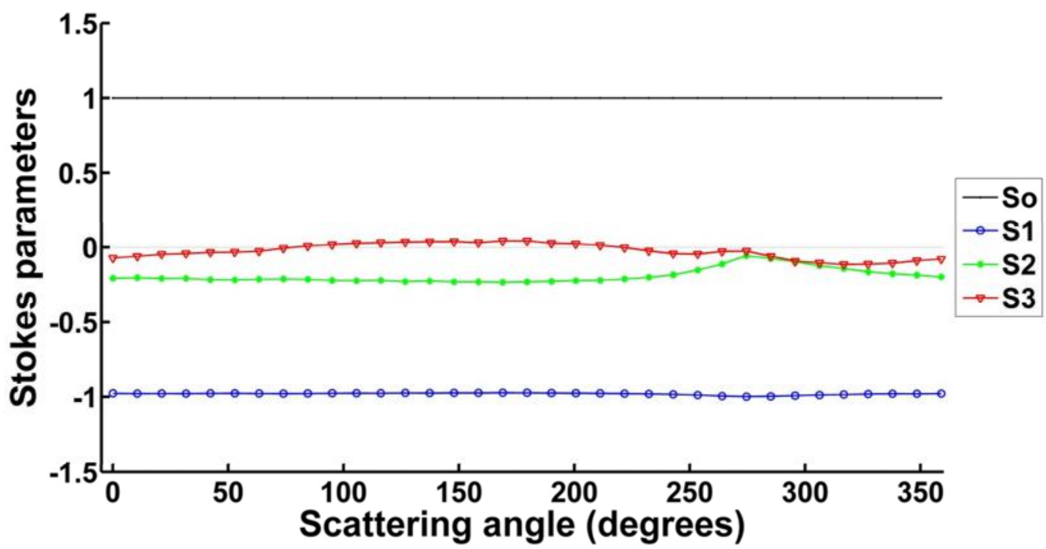

Fig. 3.1.3 Scattered Stokes parameters versus scattering angle when an aluminum cylinder is illuminated by an s-polarization state θ_0=0º and a conical angle φ=4º.

The **Fig. 3.1.4** shows a similar energy distribution when a π-polarization (p-polarization state)

state is incident in the aluminum cylinder, the most of the energy is scattered around the S_1 positive and the behavior of the rest of the Stokes vectors around the 360º are closely to the expected like the past polarization. In this case, the scattered intensities associated to +45º linear polarization are presented around the 270º where the scattered field components exhibit notable phase variations; the changes around this angle are related with the polarization of the input beam and the diffraction pattern generated in the direction of propagation of the resultant field where in that point the p polarization shows more interaction with the cylinder. The normal direction of the cylinder is perpendicular to the vector direction of the input field, the surface roughness and a possible tilt of the cylinder could be the reason of why results are present in that form, see **Fig 3.1.4**.

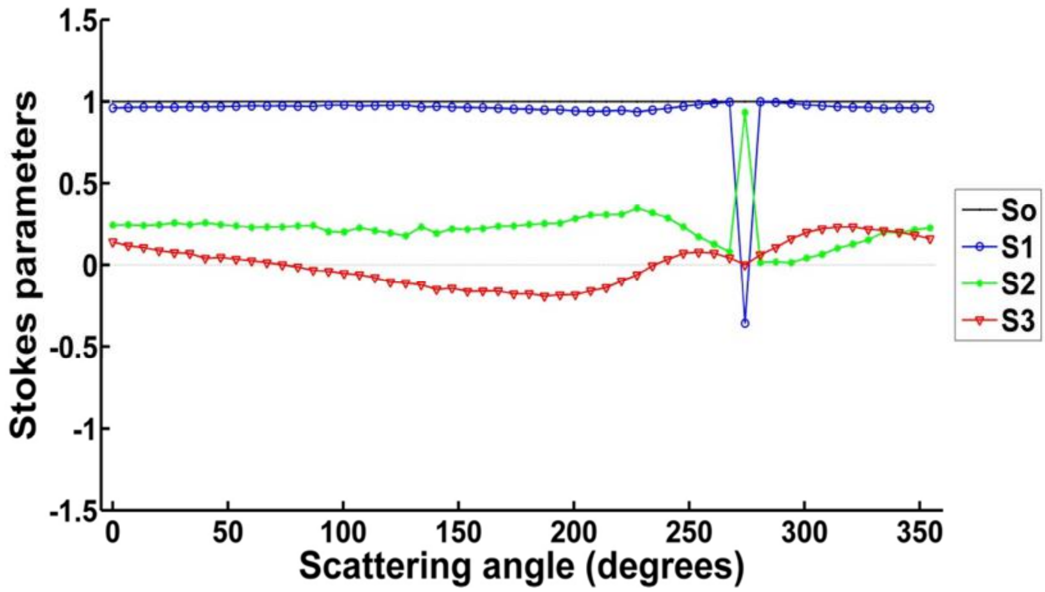

Fig. 3.1.4 Scattered Stokes parameters versus scattering angle when an aluminum cylinder is illuminated by a π-polarization state θ_0=0º and a conical angle φ=4º.

The **Fig. 3.1.5** shows a schematic representation of the angular distribution of the scattered light; The **Fig. 3.1.5 (a)** represents the angular distribution of the light scattered when a σ-polarization state is incident in the aluminum cylinder (φ=4º), which corresponds to generated unconventional radial polarization; **Fig. 3.1.5 (b)** represents the light scattered angularly when a π-polarization state is incident, where azimuthal polarization is generated.

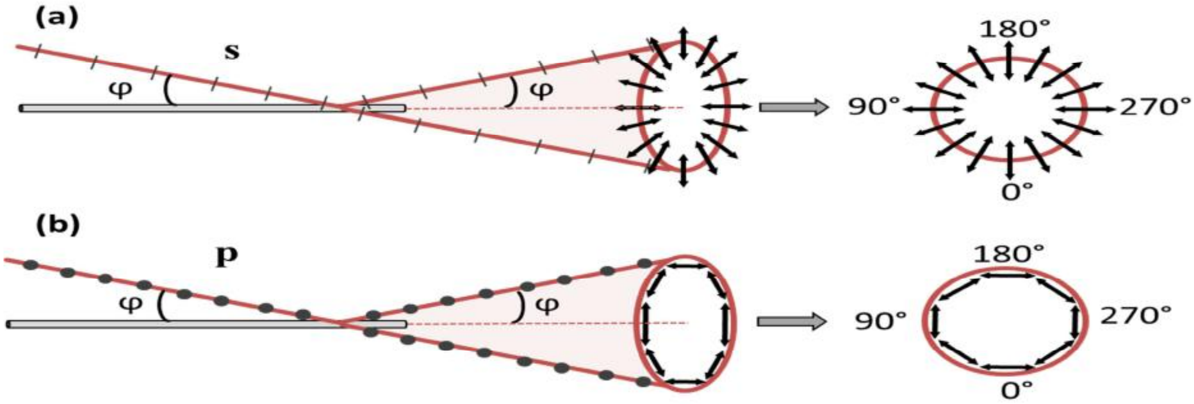

Fig. 3.1.5 Schematic representation of generation of unconventional polarization states, the thin metallic cylinder is illuminated under conical incidence. (a) s-polarization generates radial polarization. (b) p-polarization generates azimuthal polarization; φ=4º).

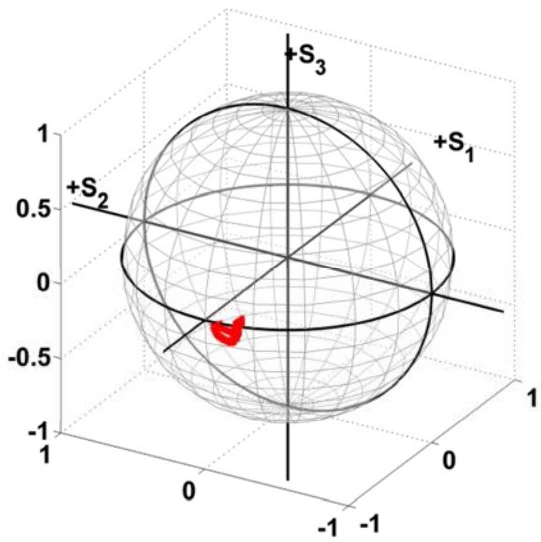

Fig. 3.1.6 Light scattered by the metallic cylinder (aluminum cylinder) when an incident beam interacts with an σ-polarization state (s-polarization state), θ_0=0º and a conical angle φ=4º; The Poincaré sphere shows the polarimetric behavior of the cylinder around the 360º.

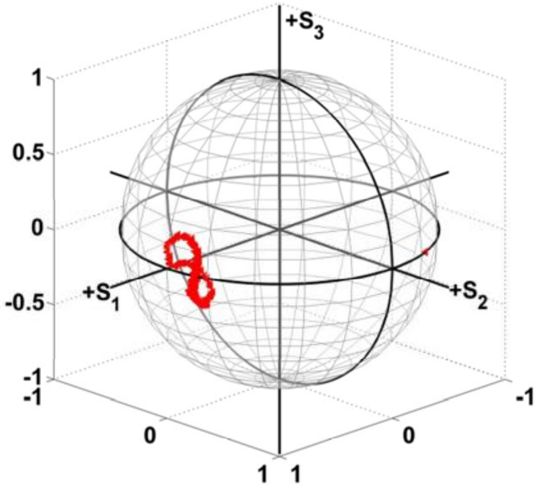

Fig. 3.1.7 Light scattered by the metallic cylinder (aluminum cylinder) when an incident beam interacts with a π-polarization state (p-polarization state), θ_0=0º and a conical angle φ=4º; The Poincaré sphere shows the polarimetric behavior of the cylinder around the 360º.

The **Figs. 3.1.6** and **3.1.7** represent the polarimetric behavior of the optical field under conical incidence; these results express the phenomena in all the light scattered angularly (360º), the Poincaré spheres give more visual information about the quality of the resultant azimuthal or radial polarization states. These results present a different distribution compared with the flat incidence, in these cases the resultant Stokes vector shows different behaviors in the optical path on the Poincaré surface, the conical incidence implies a perfect alignment, and also the cylinder tilt induce changes in the results. We have a different behavior between the s and p polarization states, where the parallel component (s polarization state) of the input beam to the cylinder normal has better response in the interaction with the cylinder, with that, the points on the Poincaré sphere have less dispersion from the representative point in the sphere that correspond to this state. In the case of a p polarization state as input beam, the points present variations around 360º, where the optical path described in the sphere shows a symmetric behavior in its distribution. In this analysis we can conclude that the π polarization state has more interaction with the cylinder, where the surface roughness and a possible tilt of the cylinder present important features in the generation of unconventional polarizations states using cylinders as generators. In the Appendix E is possible to observe small lines or roughness along to the normal axis of the cylinder (aluminum cylinder), this could be another feature that induce noise in the results.

The **Fig. 3.1.8** and **Fig. 3.1.9** show the corresponding Stokes vector around 360º when a nickel cylinder (electric guitar string) is illuminated under conical incidence through s- and p-polarization states, at an incidence angle of θ_0=0º, and conical angle φ=4.0º. It is possible to observe a similar behavior as the aluminum cylinder, where the radial polarization is generated when the incident field corresponds to s-polarization, also azimuthal polarization is generated by the incidence of p-polarization states. Based on the notation defined in **Fig. 3.1.1** for the conical geometry, the scattered light is highly associated with a p-polarization state; In this case, the scattered intensities associated to +45º linear and, slightly, to circular right and left-hand polarizations are also present in the **Appendix D**. The detector registers a maximum of approximately 270º in the direction of the propagation of the incident beam, where the scattered electric field components exhibit notable phase variations; the diffraction pattern generated by the interaction was directed in this angle, in this point we have polarimetric information even when it has more intensity than the rest of the points around the 360º.

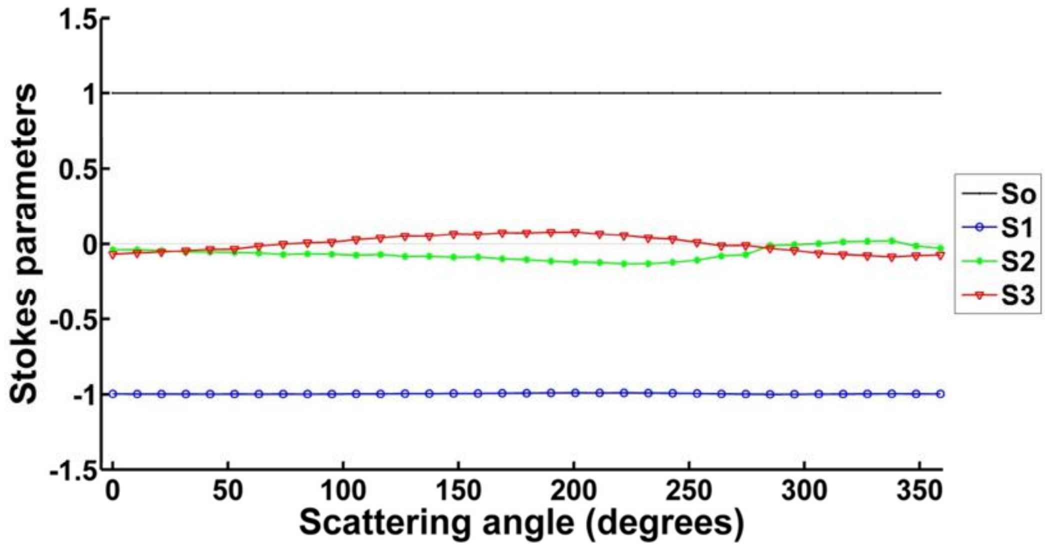

Fig. 3.1.8 Scattered Stokes parameters versus scattering angle when a nickel cylinder is illuminated by a s-polarization state θ_0=0º and a conical angle φ=4º.

The scattered Stokes parameters S_2 and S_3 have lower intensity values and are slightly less noise for the case of the nickel cylinder than the aluminum cylinder, for the same incident polarization. These results shows that the nickel cylinder has more surface roughness or defects oriented along the cylinder axis than the aluminum cylinder (aluminum evaporated on an optical fiber). This kind of superficial features found in the cylinder could be generated by the process of fabrication of the cylinder. We have observed this tendency with a high resolution microscope but we do not have exactly results from the illumination area. The images of the fiber coated with aluminum and the nickel (guitar string) were taken with a Zeiss LSM 710 NLO (Multiphoton Microscopy) [101]. They shown are in the **Appendix E**.

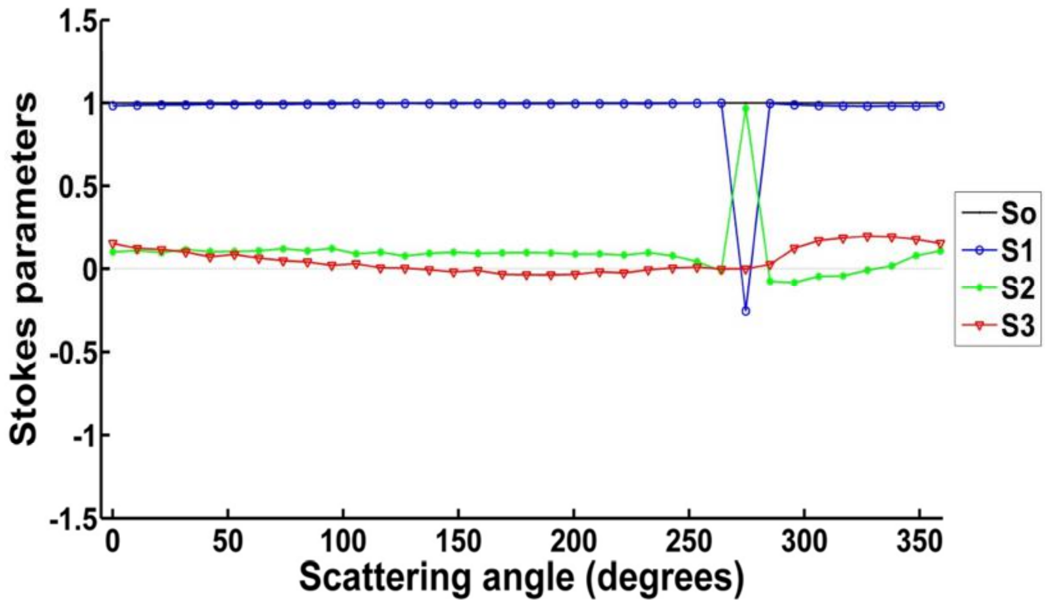

Fig. 3.1.9 Scattered Stokes parameters versus scattering angle when a nickel cylinder is illuminated by a p-polarization state θ_0=0º and a conical angle φ=4º.

A diffraction peak is present only when the polarization incident beam corresponds to the p-polarization; this is possible by an effect similar to the absorption experienced by that field by a dichroic polarizer, where the electric field is absorbed along the axis of the metallic cylinder while it is transmitted in the direction perpendicular to the axis of the metallic cylinder.

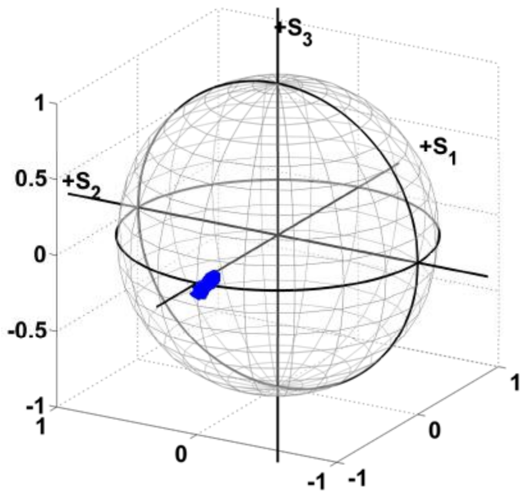

Fig. 3.1.10 Light scattered by the metallic cylinder (nickel cylinder) when an incident beam interacts with an s-polarization state (s-polarization state), θ_0=0º and a conical angle φ=4º; The Poincaré sphere shows the polarimetric behavior of the cylinder around the 360º.

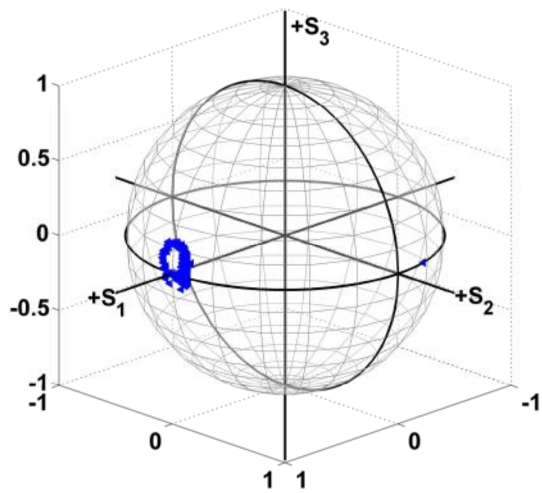

Fig. 3.1.11 Light scattered by the metallic cylinder (nickel cylinder) when an incident beam interacts with a pπ-polarization state (p-polarization state), θ_0=0º and a conical angle φ=4º; The Poincaré sphere shows the polarimetric behavior of the cylinder around the 360º.

The **Figs. 3.1.10** and **3.1.11** represent the polarimetric behavior of the optical field under conical incidence; the results express the phenomena in all light scattered angularly (360º), the Poincaré spheres give more visual information about the quality of the resultant azimuthal or radial polarization state when the light interacts with a thin nickel cylinder.

3.1.3 Discussion of the results.

A simple method to generate unconventional polarization states with radial and azimuthal symmetries has been presented. The method is based in the light scattering by thin metallic cylinders illuminated under a conical geometry; two metallic cylinders have been used: one of aluminum (optical fiber with aluminum evaporated uniformly), and the other of nickel (electric guitar string). Using appropriate and complementary elements (lenses and mirrors); this method can be used at any wavelength and applied in the surgical, industrial, and sensing fields. For example, the generated polarization states can be properly handled in the infrared region to be used as a circular cutting tool of variable diameter and ring thickness, which can be controlled through varying the metallic cylinder's diameter. To the best of our knowledge, this is the cheapest and easiest way to generate radial and azimuthal unconventional polarization states.

3.2 Angularly-resolved variable wave-retarder using light scattering from a thin metallic cylinder.

This section includes the results reported in the second article published [7] and derived from my thesis work. The ways to generate unconventional polarization states have been derived from different theories and experimental setups; this thesis work is compared with the traditional methods, where this new proposal of generation represents an important development in the vectorial optical field. The use of passive methods for generation of unconventional and conventional polarization states represent a research field that has been applied in many unsolved issues in the optics and photonics areas [30-50].

Many devices have been used with the objective to change the phase or the orthogonal components of an optical field like calcite-based linear polarizers, quartz-based retardation wave plates. Nowadays the use of electro-optic devices has been changing the way to generate polarization states like liquid crystal displays, liquid crystals on semiconductors or photoelastic modulators [38-41]. The necessity to increase the application in science of the polarized light, engineering, and photonics fields has created opportunities to explore new forms of generation of polarized light. The principal objective of the polarization equipment is just to generate any desired state (conventional or unconventional) which usually is use to illuminate a sample under study, the most common geometry applied in the experimental setups are flat in transmission or reflection; the method presented in the following sections could be useful for the generation of polarized states and applicable in any geometries of incidence. The results present experimental evidence that closed paths on the Poincarè sphere can be generated and distributed angularly with the use of a thin metallic cylinder (incidence normal or perpendicular to the cylinder axis). The experimental arrangement reported in this thesis work demonstrated that the thin cylinder behaves as a passive angularly–resolved variable wave-retarder.

In this second work, the interpretation of the polarization has to be in function of his behavior around the closed paths described on the Poincarè sphere; on the other hand, the polarization can be represented as a Stokes vector in terms of the orthogonal components of the electric field vector.

The scattering of light generated by the cylinder has been reported in both: flat and conical geometries of incidence [6 -7 and 91-97]. Even when the present phenomenon between the polarized light and the cylinder is well described in different theories and used in many applications, the complete polarization study of the scattered light by cylinders presented here, is a new and original result, which could contribute to the comprehension of geometries capable to generate phase changes within the polarized light. The objective of this section is to explain that the scattered light from a metallic cylinder (around 360º) can be used as a simple variable wave-retarder angularly-resolved.

3.2.1 Theory.

In the past sections were described the representation of the Stokes vector and its relation with the representation on the Poincarè sphere, where they can be displayed as a function of the azimuth ($0\leq 2\psi \leq 2\pi/2$) and the ellipticity ($-\pi/2\leq 2\varepsilon \leq \pi/2$) angles, defined by the Poincarè sphere (equation (3.2.1)) [12].

$$S = s_0 \begin{bmatrix} 1 \\ \cos(2\varepsilon)\cos(2\psi) \\ \cos(2\varepsilon)\sin(2\psi) \\ \sin(2\varepsilon) \end{bmatrix} = \begin{bmatrix} 1 \\ s_1 \\ s_2 \\ s_3 \end{bmatrix} \tag{3.2.1}$$

3.2.2 Methods.

The configuration of the optical system employed consists of a collimated beam of light (HeNe laser, 632.8 nm) with a 2 mm spot size; this was sent toward a metallic cylinder (nickel electric guitar string, with a 254 µm diameter). The cylinder was placed in the center of the automated rotation stage of an angle resolved scattering system (ARS; Oriel goniometer, with stepper motors), which is able to measure the polarized scattered light at each scattering angle θ_s, from 0º $\leq \theta_s \leq$ 360º, see the **Fig. 3.2.1**.

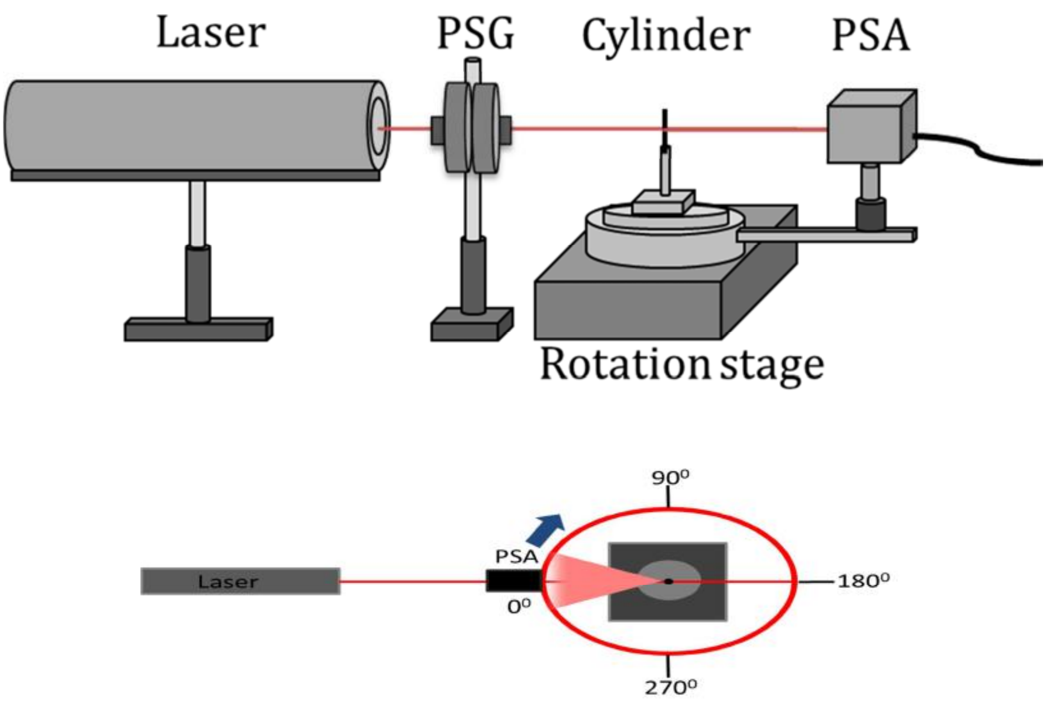

Fig. 3.2.1 Experimental setup employed for the measurement of the polarized light scattered by a metallic cylinder (nickel electric guitar string, with a 254 µm diameter). System in a flat geometry of incidence, the lower describe the methodology of measurement of the vector parameters.

The scattered light lies within a plane surface perpendicular to the cylinder axis, a set of six polarizations states: linear horizontal and perpendicular, ±45º and circular right- and left-handed were generated using a polarization state generator (PSG) and each of them was analyzed by a polarization state analyzer (PSA). The difference between these two techniques is related to the accuracy in the results, it is possible to generate more than six measurements increasing the accuracy. In our case, the quality of the generated polarization states with the PSG was the closer to the theory definition with this condition; we applied the six polarizations state method for the analysis. A PSG consists of a Glan-Thompson linear polarizer (Thorlabs, GTH10M) followed by a liquid crystal variable retarder (Thorlabs, LCC1111-A and LCC25 controlled) [99], each mounted on motorized rotations stages (Thorlabs, PRM1Z8E). The PSA consists of a combination of an achromatic rotating retarder wave-plate of $\lambda/4$, a linear polarizer and a silicon sensor as a photodetector (Thorlabs, PAX5710VIS-T), and a software program that allows the automated detection of the Stokes parameters of the scattered light [100].

The scattered Stokes vectors were measured every 1 degree and were plotted by interpolating data each 6º except around 0º (where the PSA is rotated and placed between the PSG and the cylinder, obstructing the incident light) and 180º (where the slight saturation occurs at the photodetector), all of these details are possible to see in the **Fig. 3.2.1**.

In the discussion of how the cylinder scattered the light, all of the known six basic states of polarization were generated and analyzed by the system. The linear s and p polarization states are scattered uniformly by keeping its polarization, the diffraction pattern generated by the interaction of the cylinder and the light was distributed angularly on the surface of a plane perpendicular to the cylinder. The **Fig. 3.2.2** shows the spatial energy distribution of the s-polarization state, **Fig. 3.2.5** describes the spatial energy distribution of the p-polarization. The experimental data were plotted for all the polarizations states reported as normalized scattered Stokes vectors versus the scattering angle ($0^o < \theta_s < 360^o$) and the representation of the optical path in the Poincaré sphere.

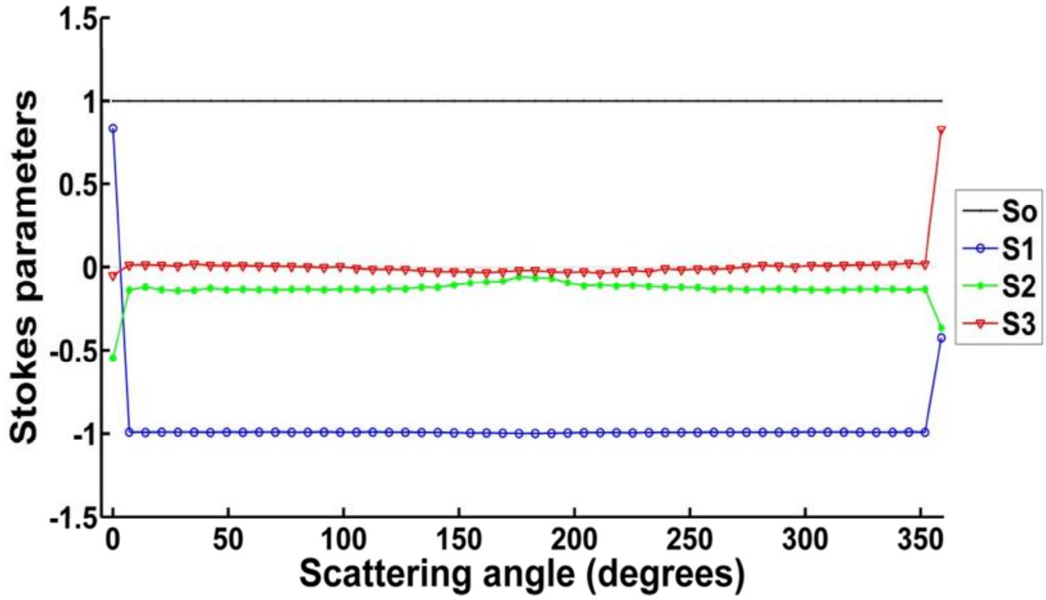

Fig. 3.2.2 Scattered Stokes parameters versus scattering angle when a nickel cylinder is illuminated by an s-polarization state in a flat incidence geometry.

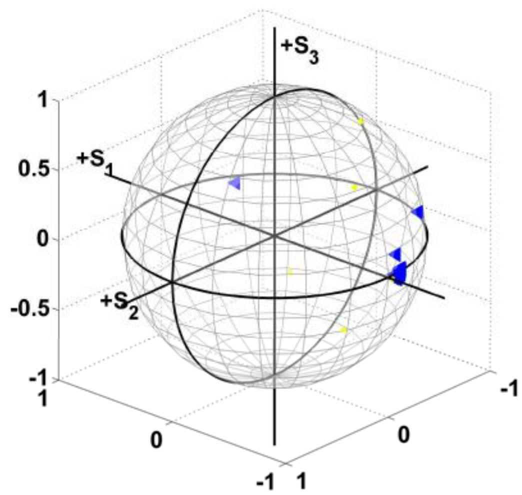

Fig. 3.2.3 Light scattered by the metallic cylinder (nickel electric guitar string), with an s-polarization state as input field perpendicularly to the cylinder axis, the Poincaré sphere representation shows the polarimetric behavior of the cylinder around the 360º.

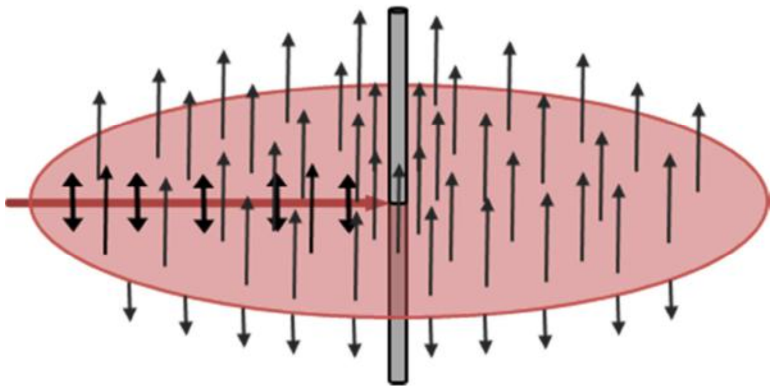

Fig. 3.2.4 Light scattered through a metallic cylinder when an incident beam with s-polarization state, artistic diagram of the scattered light distributed angularly.

In the **Fig. 3.2.2** is shown the distribution of the Stokes vectors when the incident light has an s-polarization, observe that the incident polarization never changes around the scattering angle, while the **Fig.3.2.3** represents the points in the Poincarè sphere, as it is possible to see all the points keep the same position around the scattering angle. This behavior shows that in all the points the incident polarization state keeps its polarimetric nature and then the cylinder can be used as a generator of unconventional polarization as was concluded in the past sections. The **Fig. 3.2.4** shows the light scattered by the cylinder in the entire plane. For this case the incident polarization was s-polarized.

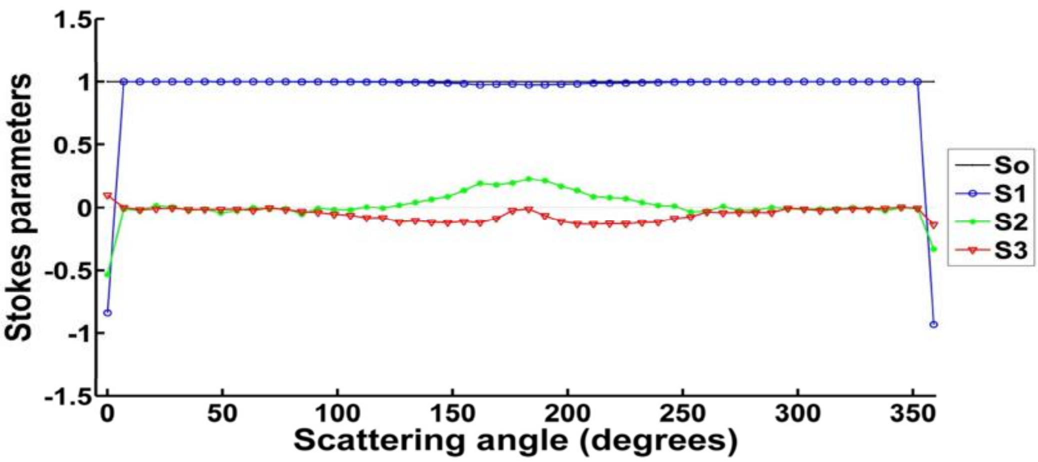

Fig. 3.2.5. Scattered Stokes parameters versus scattering angle when a nickel cylinder is illuminated by a p-polarization state in a flat incidence geometry.

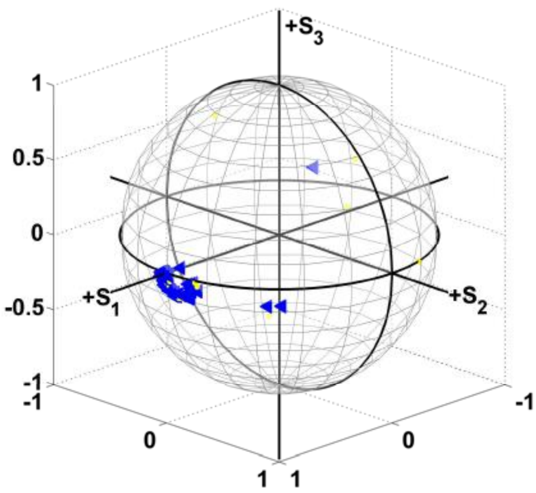

Fig. 3.2.6 Light scattered by the metallic cylinder (nickel electric guitar string), with a p-polarization state as input field perpendicularly to the cylinder axis, the Poincaré sphere representation shows the polarimetric behavior of the cylinder around the 360º.

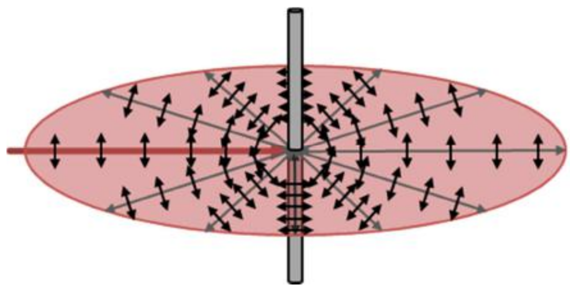

Fig. 3.2.7 Light scattered through a metallic cylinder when an incident beam with p-polarization state was sent, artistic diagram of the scattered light distributed angularly.

In the **Fig. 3.2.5** shows the distributions of the Stokes vectors when the incident light has a p-polarization, in this case around 180˚ the system presents some elliptical behavior in the resultant polarization. The **Fig. 3.2.6** represents the points in the Poincarè sphere, as it is possible to see not all the points keep the same position around the scattering angle, it is possible to explain some tilt or roughness in the surface of the cylinder are being present. The **Fig. 3.2.7** shows the light scattered by the cylinder in the entire plane. For this case the incident polarization was p-polarization.

The results obtained when the ±45˚ linear polarization states were used to illuminate the cylinder are shown in the **Figs. 3.2.8** and **3.2.10**, respectively**.** The initial points of the Stokes vectors are around the negative S_2 axis (near to θ_s=0˚) that moves gradually from the equator to the lower hemisphere, this mean the resultant field is taking elliptical left-handed polarization states, passing close to the point where it is possible to represent the circular left- polarization close to θ_s=146.7˚, the point continues its displacement until arrives to the pure +45˚ polarization state on the positive S_2 axis. This behavior corresponds to the antipodal point in the Poincaré sphere where the direction of propagation correspond to θ_s = 180˚. This behavior that is possible to observe in the Poincaré sphere is related to the ability of the cylinder to change the phase of the incident beam as a wave retarder; this is going to be discussed in the following sections and conclusions of section.

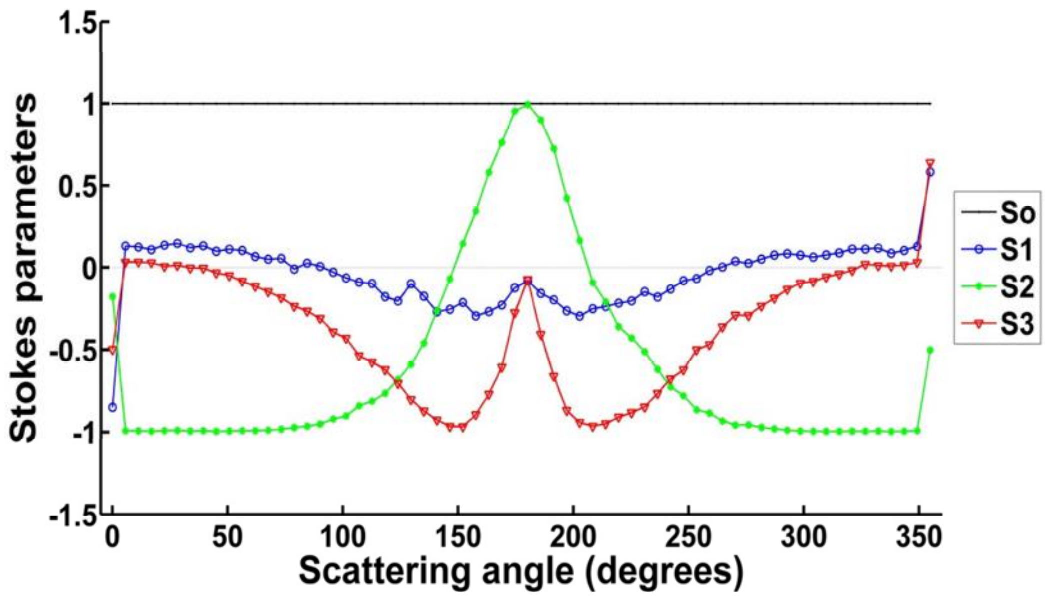

Fig. 3.2.8 Scattered Stokes parameters versus scattering angle when a nickel cylinder is illuminated by a +45º polarization state; flat incidence geometry.

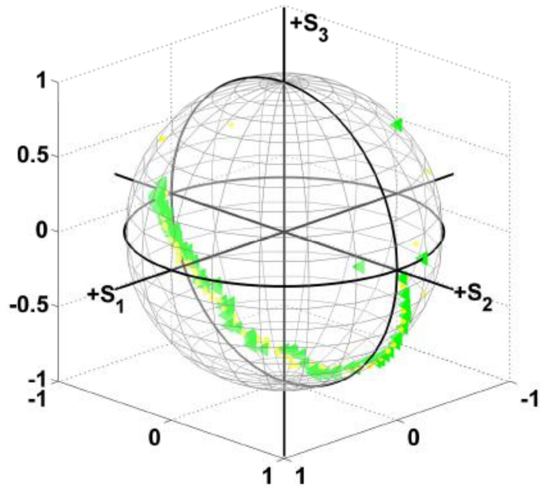

Fig. 3.2.9 Light scattered by the metallic cylinder (nickel electric guitar string), with an +45º polarization state as input field perpendicularly to the cylinder axis, and path traced on the Poincaré sphere, where the green color represents the polarized light scattered from $0^{\circ} < \theta_s < 180^{\circ}$ and the yellow color represents the polarized light scattered from $180^{\circ} < \theta_s < 360^{\circ}$.

A similar behavior but different direction of point propagation is present in the case when the incident beam has a linear -45˚ polarization (see **Fig. 3.2.10**) with the difference that the points start in the positive S_2 axis, located in the equator ($\theta_s = 0^{\circ}$).

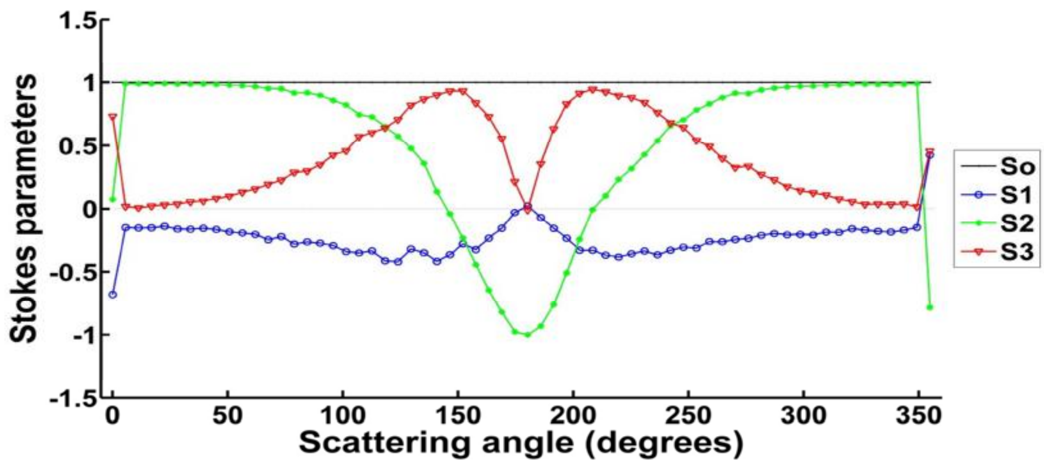

Fig. 3.2.10 Scattered Stokes parameters versus scattering angle when a nickel cylinder is illuminated by a - 45º polarization state; flat incidence geometry.

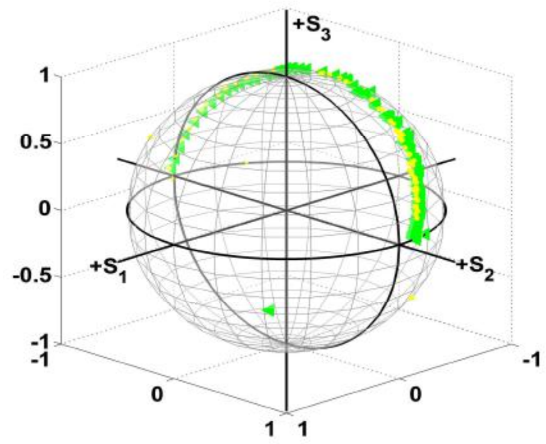

Fig. 3.2.11 Light scattered by the metallic cylinder (nickel electric guitar string), with an -45º polarization state as input field perpendicularly to the cylinder axis, and path traced on the Poincaré sphere, where the green color represents the polarized light scattered from $0^\circ < \theta_s < 180^\circ$ and the yellow color represents the polarized light scattered from $180^\circ < \theta_s < 360^\circ$.

The results obtained in the interaction between the thin cylinder and the circular left- and right-hand polarization states are shown in the next images: **Figs. 3.2.12** to **3.2.15.** The **Fig. 3.2.12** shows the incident circular right-handed polarization states, all the points have an angularly position on the Poincaré sphere, for this case the initial points are located in the negative axis of S_3 (θ_s=0˚), this means that here is present a change in phase of the incident beam, this behavior represented in the Poincaré sphere, see **Fig 3.2.13**. These points move toward to the antipodal point, located at the positive side of S_3, in this way the polarization of the resulting light takes an elliptical left-hand state passing close to the positive axis of S_2 (near θ_s=146.7˚), then resultant polarization comes close to like the incident beam at θ_s = 180˚ circular right-hand state. The **Fig. 3.2.12** shows how the symmetry is present between paths, passing through the same points like the first one nearly to +45˚ axis and finally returning to the circular left-handed polarization state.

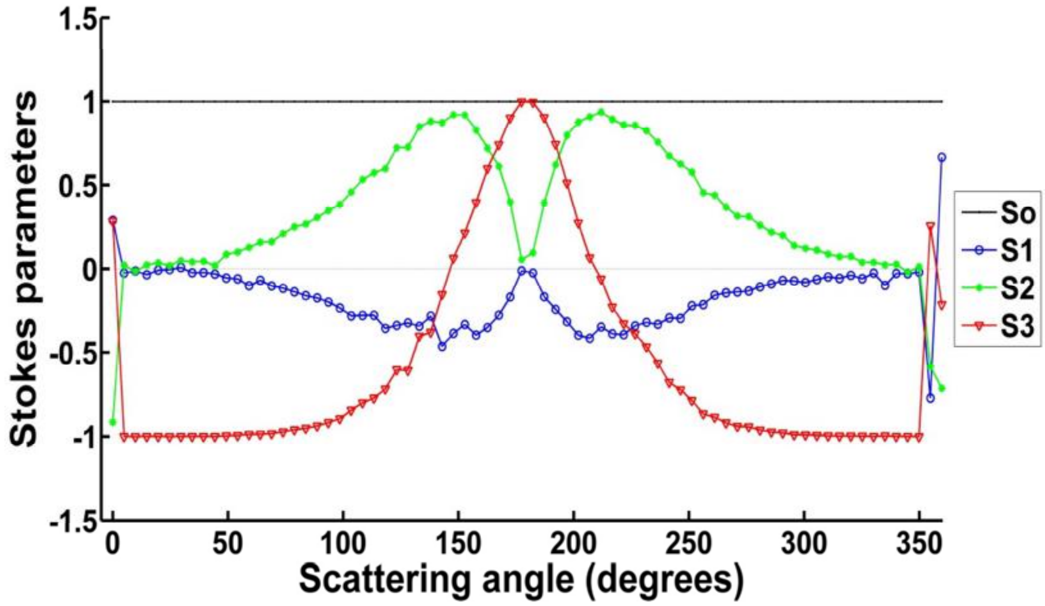

Fig. 3.2.12 Scattered Stokes parameters versus scattering angle when a nickel cylinder is illuminated by a circular right-hand polarization state in a flat incidence geometry.

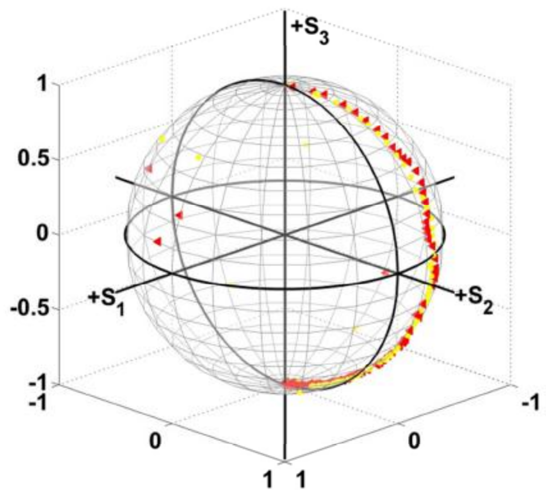

Fig. 3.2.13 Light scattered by the metallic cylinder (nickel electric guitar string), with a circular right-hand polarization state as input field perpendicularly to the cylinder axis, and path traced on the Poincaré sphere, where the red color represents the polarized light scattered from $0^{\circ} < \theta_s < 180^{\circ}$ and the yellow color represents the polarized light scattered from $180^{\circ} < \theta_s < 360^{\circ}$.

The **Fig 3.2.13** shows the optical path obtained in the analysis of the cylinder, in this representation the changes in the phase of the incident beam are more visible in all the round trip that PSA done, the changes are associate with a quarter wave plate or an half wave plates, this in different points around the scattered light by the cylinder.

For the case of the circular left-handed polarization state like incident beam the result obtained are show in the **Fig. 3.2.14** and **Fig. 3.2.15**. The paths on the Poincaré sphere beginning at the positive S_3 axis pole, then moving on the upper hemisphere, crossing the equator near to negative S_2 axis and finally arriving to negative S_3 pole (antipodal point), as it is possible to see, in all the cases are presented the same behavior but with different directions and paths in the Poincaré sphere.

In the same way that was studied the circular right- hand polarization state, the circular left-hand presented a similar behavior but in the contrary direction than the last case; the changes in phase related with a quarter wave plate ($\lambda/4$), an half wave plate ($\lambda/2$), and a lambda (λ) wave plate present this polarimetric behavior.

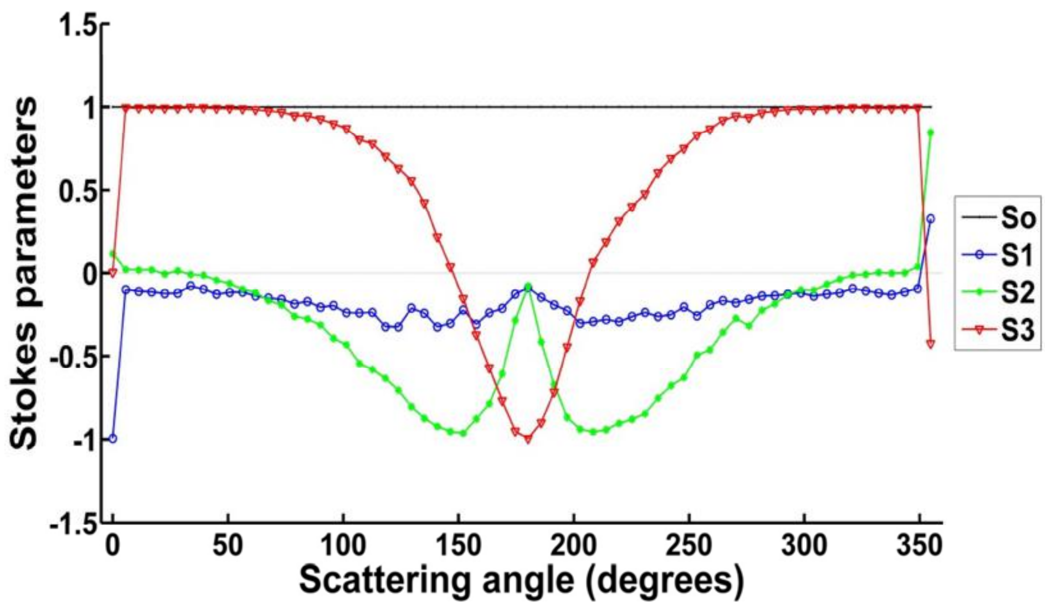

Fig. 3.2.14 Scattered Stokes parameters versus scattering angle when a nickel cylinder is illuminated by a circular left-hand polarization state in a flat incidence geometry.

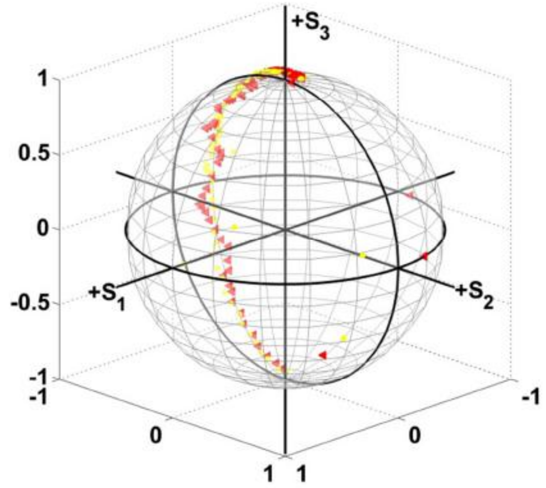

Fig. 3.2.15 Light scattered by the metallic cylinder (nickel electric guitar string), with a circular left-hand polarization state as input field perpendicularly to the cylinder axis, and path traced on the Poincaré sphere, where the red color represents the polarized light scattered from $0^{\circ} < \theta_s < 180^{\circ}$ and the yellow color represents the polarized light scattered from $180^{\circ} < \theta_s < 360^{\circ}$.

The changes between the circular right- and left- handed polarization represent a phase shift; in the case of ±45º polarized light the changes in the phase are present too. In the case of +45º, the changes are present when the resultant field switch to -45º polarization state and circular left-hand polarization state, this behavior is relate with changes in phase resolved angularly.

The paths described on the Poincarè sphere suggest a behavior related with an angularly variable wave-retarder. **Fig. 3.2.16** shows the angle-resolved wave-phase distribution associated to the light scattered when the incident polarization corresponds to a) linear ±45° and to b) circular right-handed polarization states, respectively. In order to fit the analytical expressions $S_2 = 2E_pE_s \cos\delta$ and $S_3 = 2E_pE_s \sin\delta$ with the respective experimental results, a same amplitude has been considered for the orthogonal electric field components and the same δ-phase values have been graphed for the corresponding Stokes parameters. The phase difference between the orthogonal components of the field is associated with the definition of polarization state at some point of measurement. The capability of change the phase of some material is related directly with its internal or superficial structure, the interaction of the light whit this systems generate changes in the resultant polarizations state. The phase difference between the orthogonal components of the field is associated with the definition of polarization state at some point of measurement. The capability of change the phase of some materials is related directly with its internal or superficial structure, these mediums generates changes in the resultant polarizations state; in our case the cylindrical symmetry, the study around 360º of scattered light, and the complete polarimetric study. Note the cylinder, indeed behaves as an angularly-resolved wave-retarder, where $0° \leq \delta (\theta_s) \leq 180°$, whose birefringent axis is located along its own axis.

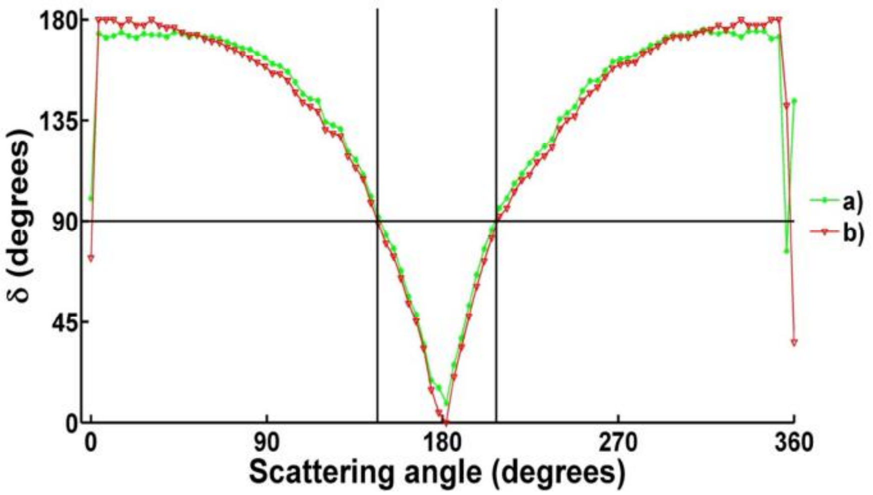

Fig. 3.2.16. Angle-resolved wave-retarder distribution $\delta(\theta_s)$ when the polarization incident is (a) +45˚ polarization state and (b) circular right-handed polarization state.

3.2.3 Discussion of the results.

An experimental analysis of the angularly scattered polarized light by a thin metallic cylinder has been presented herein by using the Stokes and the Poincarè sphere formalisms. The results show that the incident linear s- and p-polarized states do not change under the scattering in a planar geometry of incidence. On the other hand, the incident linear +45º, -45º, circular right-, and left-handed polarization states, respectively, are scattered with a uniform intensity, but with angularly variable polarization states. The complete scattered polarization states can be represented as points that describe closed-paths on the Poincarè sphere, where the initial and the returning points are antipodal polarization states one from the other. These results can be extrapolated to other possible incident polarization states, which surely will have associated different closed-paths on the Poincarè sphere, with initial and returning points corresponding to antipodal polarization states. This means, a thin metallic cylinder operates as an angularly-resolved variable wave-retarder that can be used as an angularly-selective state of polarization generator. Consequently, the thin metallic cylinder surface may be tailored properly to handle the distribution of light (with collimated, focused or diverging energy distributions) and its associated polarization properties. Several useful devices could be constructed based in this easy, cheap, and controllably method. With the aid of proper reflecting or refracting optics, several designs can be employed as planar illuminators with desired spatially tailored energy and polarization distributions.

Chapter 4

4.1 General conclusions.

The experimental results generated by the interaction between conventional polarized light and a thin metallic cylinder under both, a conical and a plane-of-incidence geometry, respectively, have been presented. A simple form to generate radial and azimuthal polarization states has been proposed, such method is able to work with different wavelengths, different diameters and materials of the cylinder, in free space and to our knowledge, and it is the cheapest and easiest method to generate these unconventional polarization states. On the other hand, also a simple method to generate a wave-retarder resolved angularly was proposed, using an in plane-of-incidence geometry for the polarized light scattered by a metallic cylinder.

- In the first experimental setup were selected two different cylinders as 1-D systems: a silver-coated thin film on an optical fiber and a nickel cylinder (an electric guitar string), respectively.
- A new method, capable to generate unconventional polarization states with the interaction between a thin metallic cylinder and two kinds of conventional polarizations states: horizontal and vertical polarized light. This experimental setup was developed under a conical configuration.
- The Stokes vector representation of the data originated from the experimental setup (conical and flat) along of the full circle (360º) represents a direct way to see how the cylinder changes the polarizations angularly.
- The polarimetric behavior derived from the data was represented in the Poincaré sphere; which offered an easy way to observe the polarized light scattered angularly (the tendency to follow a symmetric pattern around antipodal points located at the basic polarization states).
- The incidence of conventional polarized light in a flat configuration shows that the thin nickel cylinder can be used as a wave plate retarder resolved angularly, with phase shifts of $\lambda/2$, $\lambda/4$.
- The possibility to have a wave plate retarder capable of work in a big range of

wavelengths represents an important tool in the optics and photonics laboratories, and now this problem is solved with the use of a thin cylinder and selecting the proper polarized light.

- There are many studies related with the use of polarized light as an inspection toot to characterize samples under any of the polarimetric formalisms; however, nobody had done before us a complete polarimetric analysis of the polarized light scattered by a cylinder, and even nobody had used it as a generator of unconventional polarized light.
- With the correct election of the cylinder and the appropriate wavelength, this kind of generators could be applied in real problems. The facility and low price of this technique makes more interesting and with a big branch of possible applications in many fields of the optics and photonics.

4.2 Future work.

The majority of the scientific references make emphasis in the use of polarization as a method of analysis of mediums or samples, but when the quality of the information increases in importance and applicability, the increasing on the resolution of a microscope for example, the polarized light analysis becomes a very important tool in the science. In all the Optical laboratories the polarized light is present; nowadays the introduction of new analyses are under the focus of unconventional polarization states has been increasing.

The optical tweezers use a specific polarization state, according their application, where the radial and azimuthal polarization states are useful because they have associated a momentum implicitly. Our generator of unconventional states can be used in a microscopic setup with the objective to be used as a new way to control the particles.

The increase in the biological applications related with studies applied to the human skin with the objective to solve problems related with detection of possible problems in the skin where the unconventional polarization states are used as a form of analysis, our experimental system could be used as a cheap and easy form to generate this kind of polarization states, the capability to make a complete analysis of the skin using different wavelengths.

In general, the use of unconventional polarization in optical fibers, optic microscope, interferometric systems, laser cut equipment, optical coherence tomography, medicine, and weather prediction are used as polarimetric characterization of the medium; all of these possible applications add importance to our methods of generation of unpolarized light and as a variable-retarder solved angularly tool.

References

1. Zeng Nan, Jiang Xiaoyu, Gao Qiang, He Yonghong, and Ma Hui. Linear polarization difference imaging and its potential applications, Applied Optics **48** (35), 6734-6739 (2009).
2. Jihoon Kim, Junghwan Oh, Hyun Wook Kang, Ho Lee, Jeehyun Kim. Detection of Tendon Tears by Degree of Linear Polarization Imaging. Journal of Optical Society of Korea **13** (4), 472-477 (2009).
3. Qiwen Zhan, Trapping metallic Rayleigh particles with radial polarization, Optics Express **12** (15), 3377-3382 (2004).
4. Haiyan Wang, Guanghao Rui, Qiwen Zhan, Dynamic propagation of optical vortices embedded in full Poincaré beams with rotationally polarization symmetry, Optics Communications **351,** 15-25 (2015).
5. Martin Kraus, Marwan Abdou Ahmed, Andreas Michalowski, Andreas Voss, Rudolf Weber, and Thomas Graf, Microdrilling in steel using ultra short pulsed laser beams with radial and azimuthal polarization, Optics Express **18** (21), 22305-22313 (2010).
6. Izcoatl Saucedo-Orozco, Guadalupe López-Morales, and R. Espinosa-Luna, Generation of unconventional polarization from light scattered by metallic cylinders under conical incidence, Optics Letters **39** (18), 5341-5344 (2014).
7. Izcoatl Saucedo-Orozco, Rafael Espinosa-Luna, and Qiwen Zhna, Angularly-resolved variable wave-retarder using light scattering from a thin metallic cylinder, Optics Communications **352**, 135-139 (2015).
8. W. Han, Y. Yang, W. Chen, Q. Zhan, Vectorial optical field generator for the creation of arbitrary complex fields, Optics Express **21** (18), 20692-20706 (2013).
9. http://www.arcoptix.com/radial_polarization_converter.htm, for more information about the optical generator of unconventional polarization.
10. R. M. A. Azzam and N.M. Bashara, Ellipsometry and Polarized light, North-Holland (1989).
11. Max Born, Emil Wolf, Principle of Optics. Seven Edition, Cambridge University, (1999).
12. Dennis Goldstein, Polarized Ligth, Second Edition, CRC Press, Florida U.S.A. 22-105. (2003).

13. Edward Collett, Field guide to polarization, SPIE (2009).
14. Moti Firdman, Micha Nixon, Eran Grinvald, Nird Davison, and Asher A. Friesem, Optics Express **18** (10), 10805-10812 (2010).
15. J. Scott Tyo, Dennis L. Goldstein, David B. Chenault, and Joseph A. Shaw, Review of passive imaging polarimetry for remote sensing applications, Applied Optics **45** (22), 5453-5469 (2006).
16. Blair A. Barbour, Howard B. Barnes, Charles P. Lewis, Patricia E.A Lindquist, Michael W. Jones, and Neil Mohon, Applications of generation images where contrast is small, Optics and Photonics News, August, 45-48 (1998).
17. S. G. Demos, and R. R. Alfano, Optical polarization imaging, Applied Optics **36** (1), 150-155 (1997).
18. A. Skumanich and B. W. Lites, Stokes profile analysis and vector magnetic fields. I. Inversion of photospheric lines, The Astrophysical Journal **322,** 473-482 (1987).
19. Nirmalya Ghosh, and I. Alex Vitkin, Tissue polarimetry: concepts, challenges, applications, and outlook, Journal of Biomedical Optics **16** (11), Art. 1108011- 29 (2011).
20. Steven L. Jacques, Jessica C. Ramella-Roman, and Ken Lee, Imaging skin pathology with polarized light, Journal of Biomedical Optics **7** (3), 329-340 (2002).
21. Jihoon Kim, Junghwan Oh, Hyun Wook Kang, Ho Lee, and Jeehyun Kim, Detection of tendon tears by degree of linear polarization imaging, Journal of Optical Society of China **13** (4), 472-477 (2009).
22. Russel A. Chipman, Ch. 22 Polarimetry, Handbook of Optics, Journal of the Optical Society of America **2**, 22.1-22.37 (1995).
23. R. Espinosa-Luna, G. Atondo-Rubio, E. Bernabeu, and S. Hinojosa-Ruiz, Dealing depolarization of light in Mueller matrices with scalar metrics, Optik **121,** 1058-1068 (2010).
24. Zhi-Cheng Ren, Ling-Jun Kong, Si-Min Li, Sheng-Xia Qian,Yongnan Li, Chenghou Tu, and Hui-Tian Wang, Generalized Poincaré sphere, Optics Express **23** (20), 26586-26595 (2015).
25. Krzysztof Perlicki, Polarization configuration recognition based on analysis of torsion

and curvature, Optics Communications **264,** 70-76 (2006).

26. Razvigor Ossikovski, José J. Gil, and Ignacio San José, Poincaré sphere mapping by Mueller matrices, Journal of the Optical Society of America **30** (11), 2291-2305 (2013).
27. Haiyan Wang, Guanghao Rui, and Qiwen Zhan, Dynamic propagation of optical vortices embedded in full Poincaré beams with rotationally polarization symmetry, Optics Communications **351**, 15-25 (2015).
28. Qiwen Zhan, Vectorial optical fields, first edition, World Scientific, 1-10 (2014).
29. Qiwen Zhan, Focus issue: unconventional polarization states of light, Optics Express **18** (10), 10775- 10776 (2010).
30. Qiwen Zhan, Cylindrical vector beams: from mathematical concepts to applications, Advances in Optics and Photonics **1,** 1-57 (2009).
31. Yuichi Kozawa and Shunichi Sato, Generation of a radially polarized laser beam by use of a conical Brewster prism, Optics Letters **30** (22), 3063-3065 (2005).
32. Kazuhiro Yonezawa, Yuichi Kozawa, and Shunichi Sato, Compact laser with radial polarization using birefringent laser medium, The Japan Society of Applied Optics **46** (8a), 5160-5163 (2007).
33. Michael R. Beversluis and Lukas Novotny, Programmable vector point-spread function engineering, Optics Express **14** (7), 2650-2656 (2006).
34. Wei Han, Yanfang Yang, Wen Cheng, and Qiwen Zhan, Vectorial optical field generator for the creation of arbitrarily complex fields, Optics Express **21** (18), 20692-20705 (2013).
35. Zhizhong Zhuang, Seong-Woo Suh, and J. S. Patel, Polarization controller using nematic liquid crystals, Optics Letters **24** (10), 694-696 (1999).
36. Ignacio Moreno, Jeffrey A. Davis, Taylor Womble-Dahl, and Don M. Cottrell, Azimuthal multiple beam interference effects with combinations of vortex beams, Optics Express **40** (10), 2341-2344 (2015).
37. Siddharth Ramachandran, Poul Kristensen, and Man F. Yan, Generation and propagation of radially polarized beams in optical fibers, Optics Letters **34** (16), 2525- 2527 (2009).
38. T. Grosjean, D. Courjon, M. Spajer, An all-fiber for generating radially and other polarized light beams, Optics Communications **203,** 1-5 (2002).

39. Xi-Lin Wang, Jianping Ding, Wei-Jiang Ni, Cheng-Shan Guo, and Hui-Tian Wang, Generation of arbitrary vector beams with a spatial light modulator and a common path interferometric arrangement, Optics Letters **32** (24), 3549-3551 (2007).
40. R Liu, D B Phillips, F Li, M D Williams, D L Andrews, and M J Padgett, Discrete emitter as a source of orbital angular momentum, Journal of Optics **17,** 1-7 (2015).
41. Gianluca Ruffato, Michele Massari, Marta Carli, and Filippo Romanato, Spiral phase plates with radial discontinuities for the generation of multiring orbital angular momentum beams: fabrication, characterization, and application, Optical Engineering **54** (11), Art. 1113071-7 (2015).
42. Galina Machavariani, Yaakov Lumer, Inon Moshe, Avi Meir, Steven Jackel, and Nir Davidson, Birefringence-induced bifocusing for selection of radially or azimuthally polarized laser modes, Applied Optics **46** (16), 3304-3310 (2007).
43. Reza Aghbolaghi and Habib Sahebghoran Charehjolo, Radially and azimuthally polarized laser beams by thin-disk laser, Applied Optics **55** (13), 3510- 3517 (2016).
44. Tobias Ehmke, Tim Heiko Nitzsche, Andreas Knebl, and Alexander Heisterkamp, Molecular orientation sensitive second harmonic microscopy by radially and azimuthally polarized light, Biomedical Optics Express **5** (7), 2231- 2246 (2014).
45. Jing Li, and Xiaoping Wu, FDTD simulation of trapping nanowires with linearly polarized and radially polarized optical tweezers, Optics Express **19** (21), 20736- 20742 (2011).
46. Yaoju Zhang, Yuxing Dai, Multifocal optical trapping using counter-propagating radially-polarized beams, Optics Communications **285,** 725-730 (2012).
47. Praveen C Ashok and Kishan Dholakia, Optical trapping for analytical biotechnology, Current Opinion in Biotechnology **23,** 16-21 (2012).
48. Youyi Zhuanga, Yaoju Zhanga, Biaofeng Dinga, Taikei Suyamab, Trapping Rayleigh particles using highly focused higher-order radially polarized beams, Optics Communications **284** (7), 1734-1739 (2011).
49. T. W. Ebbesen, H. J. Lezec, H. F. Ghaemi, T. Thio, P. A. Wolff, Extraordinary optical transmission through sub-wavelength hole arrays, Nature **391,** 667-669 (1998).
50. P. Banzer, J. Kindler (nee M´ uller), S. Quabis, U. Peschel, and G. Leuchs, Extraordinary

transmission through a single coaxial aperture in a thin metal film, Optics Express **18** (10), 10896-10904 (2010).

51. Pavel Ginzburg, Amir Nevet, Nikolai Berkovitch, Alexander Normatov, Gilad M. Lerman, Avner Yanai, Uriel Levy, and Meir Orenstein, Plasmonic Resonance Effects for Tandem Receiving-Transmitting Nanoantennas, Nano Letters **11,** 220-224 (2011).
52. Guanghao Rui, Weibin Chen, and Qiwen Zhan, High efficiency plasmonic probe design for parallel near-field optics applications, Optics Express **19** (6), 5187- 5195 (2011).
53. Ricardo A. Depine, Antispecular enhancement in s- and p-polarized electromagnetic waves scattered from random gratings, Optics Express **16** (19), 1457- 1459 (1991).
54. R. E. Luna, Scattering by one-dimensional random rough metallic surface in a conical configuration: several polarizations, Optics Letters **21** (18), 1418- 1420 (1996).
55. I. V. Novikov and A. A. Maradudin, The Stokes matrix in conical scattering from a one-dimensional perfectly conducting randomly rough surface, Radio Science **34,** 599-609 (1999).
56. Rafael Espinosa-Luna, Scattering by rough surface in a conical configuration: Experimental Mueller matrix, Optics Letters **27** (17), 1510-1512 (2002).
57. N. C. Bruce, Kirchhoff calculations of the coherent scatter from a series of very rough surfaces, Applied Optics **34** (24), 5531- 5536 (1995).
58. N. C. Bruce and J. C. Dainty, Multiple scattering from rough dielectric and metal surfaces using the Kirchhoff approximation, Journal of Modern Optics **38** (8), 1471-1481 (1991).
59. K. A. O'Donnell and M. E. Knotts, Polarization dependence of scattering from one-dimensional rough surfaces, Journal of the Optical Society of America **8** (7), 1126-131 (1991).
60. A. D. Arsenieva, A. A. Maradudin, Jun Q. Lu, and A. R. McGurn, Scattering of light from random surfaces that are periodic on average, Optics Letters **18** (19), 1588-1590 (1993).
61. Myriam Zerrad, Jacques Sorrentini, Gabriel Soriano, and Claude Amra, Gradual loss of polarization in light scattered from rough surfaces: Electromagnetic prediction, Optics Express **18** (15), 15832-15843 (2010).

62. Claude Amra, C. Grezes-Besset, and L. Bruel, Comparison of surface and bulk scattering in optical multilayers, Applied Optics **32** (28), 5492-5503 (1993).
63. S-waveplate (Radial Polarization Converter) from Altechna. http://www.altechna.com
64. Rudolf Weber, Andreas Michalowski, Marwan Abdou-Ahmed, Volkher Onuseit, Volker Rominger, Martin Kraus, Thomas Graf, Effects of Radial and Tangential Polarization in Laser Material Processing, ScienceDirect **12,** 21–30 (2011).
65. Martin Kraus, Marwan Abdou Ahmed, Andreas Michalowski, Andreas Voss, Rudolf Weber, and Thomas Graf, Microdrilling in steel using ultrashort pulsed laser beams with radial and azimuthal polarization, Optics Express **18** (21), 22305- 22313 (2010).
66. O J Allegre, W Perrie, S P Edwardson, G Dearden and K G Watkins, Laser microprocessing of steel with radially and azimuthally polarized femtosecond vortex pulses, Journal of Optics **14,** Art. 085601 (2012).
67. Baoxian Zhang, Zhaozhong Chen, Hao Sun, Jianpei Xia and Jianping Ding, Vectorial optical vortex filtering for edge enhancement, Journal of Optics **18,** Art. 035703 (2016).
68. R. Dorn, S. Quabis, and G. Leuchs, Sharper Focus for a Radially Polarized Light Beam, Physics Letters **91** (23), 233901-233904 (2003).
69. Stephen D. Grant, Svetlana A. Zolotovskaya, W. Allan Gillespie, Todor K. Kalkandjiev,2 and Amin Abdolvand, Azimuthally and radially polarized light in conical diffraction, Optics Letters **39** (7), 1988- 1991 (2014).
70. Wenjing Zhang, Xuanzhe Zhang, Yu Cao, Haibo Liu, and Zejin Liui, Robust sky light polarization detection with an S-wave plate in a light field camera, Applied Optics **55** (13), 3518-3525 (2016).
71. Aidas Matijošius, Paulius Stanislovaitis, Titas Gertus, Valerijus Smilgevičius, Formation of second order optical vortices with a radial polarization converter using the double-pass technique, Optics Communications **349,** 24-30 (2015).
72. Aidas Matijošius, Paulius Stanislovaitis, Titas Gertus, Valerijus Smilgevičius, Formation of optical vortices with topological charge |1|= 1and |l| =1/2 by use of the S-waveplate, Optics Communications **324,** 1-9 (2014).
73. M. Nieto-Vesperinas and J. M. Soto-Crespo, Monte Carlo simulations for scattering of electromagnetic waves rom perfectly conductive random rough surfaces, Optics Letters

12 (12), 979-981 (1987).

74. M.-J. Kim, J. C. Dainty, A. T. Friberg, and A. J. Sant, Experimental study of enhanced backscattering from one- and two-dimensional random rough surfaces, Journal of the Optics Society of America A **7** (4), 569-577 (1990).
75. E. R. Méndez, M. A. Ponce, V. Ruiz-Cortes, and Zu-Han Gu, Photofabrication of one-dimensional rough surfaces for light-scattering experiments, Applied Optics **30** (28), 4103- 4112 (1991).
76. José J. Gil1, and Ignacio San José, Polarimetric subtraction of Mueller matrices, Journal of the Optical Society of America A **30** (6), 1078-1088 (2013).
77. F. J. García-Vidal, and L. Martín-Moreno, Transmission and focusing of light in one-dimensional periodically nanostructured metals, Physics Review B **66,** Art. 155412 (2012).
78. K. A. O'Donnell and M. E. Knotts, Polarization dependence of scattering from one-dimensional rough surfaces, Journal of the Optical Society of America A **8** (7), 1126-1131 (1991).
79. N.C. Bruce, A.J. Sant, J.C. Dainty, The Mueller matrix for rough surface scattering using the Kirchhoff approximation, Optics Communications **88,** 471-484 (1992).
80. T. R. Michel, M. E. Knotts, and K. A. O'Donnell, Stokes matrix of a one-dimensional perfectly conducting rough surface, Journal of the Optical Society of America A **9** (4), 585-596 (1992).
81. M. E. Knotts, T. R. Michel, and K. A. O'Donnell, Comparisons of theory and experiment in light scattering from a randomly rough surface, Journal of the Optical Society of America A **10** (5), 928-941 (1993).
82. Gelacio Atondo-Rubio, Rafael Espinosa-Luna, Alberto Mendoza-Suárez, Mueller matrix determination for one-dimensional rough surfaces with a reduced number of measurements, Optics Communications **244,** 7-13 (2005).
83. Foeke Kuik, Johan F. de Haan, and Joop W. Hovenier, Single scattering of light by circular cylinders, Applied Optics **33** (21), 4906- 4918 (1994).
84. D. Felbacq, G. Tayeb, and D. Maystre, Scattering by a random set of parallel cylinders, Journal of the Optical Society of America A **11** (9), 2526- 2538 (1994).

85. C. Sönnichsen, T. Franzl, T. Wilk, G. von Plessen, and J. Feldmann, Drastic Reduction of Plasmon Damping in Gold Nanorods, Physics Review **88** (7), Art. 077402 (2002).
86. A. Kienle, F. K. Forster, and R. Hibst, Anisotropy of light propagation in biological tissue, Optics Express **29** (22), 2617-2619 (2004).
87. Catherine J. Murphy, Anand M. Gole, Simona E. Hunyadi, and Christopher J. Orendorff, One-Dimensional Colloidal Gold and Silver Nanostructures, Inorganic Chemistry **45** (19), 7544-7554 (2006).
88. Siu-Chun Lee, Scattering by a dense finite layer of infinite cylinders at oblique incidence, Journal of the Optical Society of America A **25** (10), 2489- 2498 (2008).
89. H. C. Van der Hulst, Light Scattering by Small Particles (Dover, Amsterdam, 1957).
90. Gorden Videen and Dat Ngo, Light scattering from a cylinder near a plane interface: theory and comparison with experimental data, Journal of the Optical Society of America A **14** (1), 70- 78 (1997).
91. J. M. Saiz, P. J. Valle, F. Gonzalez, E. M. Ortiz, and F. Moreno, Scattering by a metallic cylinder on a substrate: burying effects, Optics Letters **21** (17), 1330- 1332 (1996).
92. Luis Miguel Sanchez-Brea, Philip Siegmann, Maria Aurora Rebollo, and Eusebio Bernabeu, Optical technique for the automatic detection and measurement of surface defects on thin metallic wires, Applied Optics **39** (4), 539- 545 (2000).
93. Eusebio Bernabeu, Ibrahim Serroukh, Luis Miguel Sanchez-Brea, Geometrical model for wire optical diffraction selected by experimental statistical analysis, Optical Engineering **38** (8), 1319–1325 (1999).
94. Luis Miguel Sanchez-Brea, Eusebio Bernabeu, Diffraction by cylinders illuminated in oblique, off-axis incidence, Optik **112** (4), 169–174 (2001).
95. Soraya A. Khodier, Measurement of wire diameter by optical diffraction, Optics Communications **36,** 63 – 67 (2004).
96. Jinhuan Li, Osami Sasaki, Takamasa Suzuki, Measurement of diameter of metal cylinders using a sinusoidally vibrating interference pattern, Optics Communications **260**, 398-402 (2006).
97. Luis Miguel Sanchez-Brea, Diffraction of cylinders with longitudinal surface structures, Journal of the Optical Society of America A **21** (6), 1102-1108 (2004).

98. ThorLabs, Half-wave LC retarder, wavelength range from 350 to 700 nm. https://www.thorlabs.de/thorproduct.cfm?partnumber=LCC1111-A
99. ThorLabs, Liquid crystal controller. https://www.thorlabs.com/thorproduct.cfm?partnumber=LCC25
100. ThorLabs, Polarimeter Module with External Sensor, 400 - 700 nm, https://www.thorlabs.com/thorProduct.cfm?partnumber=PAX5710VIS&pn=PAX5710VIS#4710
101. Zeiss LSM 710 NLO (Multiphoton Microscopy). http://www.zeiss.com/microscopy/int/home.html

Appendix A

In this section of the thesis we are going to present the corresponding programs developed in MatLab for the presentation and analysis of the results presented in the previous sections and Chapters. For this part, the deduction of the Stokes vectors from the interaction between the incident beam and the thin cylinder are presented in all the measurements.

```
clc
close all
clear all

% FLAT AND CONICAL INCIDENCE
% In this program we will describe the polarization response represented as
% Stokes vector when the light pass through a thin cylinder, the
% representation of the results correspond % of a graphical that shows the
% polarimetric behavior around 360º.


% Experimental data
% Input data (S and P polarization states)
% It is important to mention that all of the data generated by the
% interaction were saved and loaded later for the complete analysis

Sp = csvread('p.csv',24,0);
tp = Sp(1:1024,1);
powerp = Sp(1:1024,11);

Ss = csvread('s.csv',24,0);
ts = Ss(1:1024,1);
powers = Ss(1:1024,11);
```

```
% Input data for the P polarization as an incident beam

DoP = Sp(1:1024,9);
Sout0p = ones(1024,1);
Sout1p = Sp(1:1024,2);
Sout2p = Sp(1:1024,3);
Sout3p = Sp(1:1024,4);

% Input data for the S polarization as an incident beam

DoP = Ss(1:1024,9);
Sout0s = ones(1024,1);
Sout1s = Ss(1:1024,2);
Sout2s = Ss(1:1024,3);
Sout3s = Ss(1:1024,4);

Conversion from dBm to mW
powerp = 10.^(powerp/10);
powers = 10.^(powers/10);
Gr = 0:450/(1024-1):450;
%
SresS = horzcat(Sout0p,Sout1p,Sout2p,Sout3p);
SresP = horzcat(Sout0s,Sout1s,Sout2s,Sout3s);
A=(0:1024);
A=A.*0;

% Plotting

figure(1);
```

```
paso = 1:30:1024;
plot(Gr(paso),Sout0s(paso),'.-k',Gr(paso),Sout1s(paso),'-ob',Gr(paso),Sout2s(paso),'-
g*',Gr(paso),Sout3s(paso),'-rv','linewidth',1.4)
hold on
plot(Gr(1:1024),A(1:1024),':k','linewidth',0.5)
hold off

title('Conicalincidence.Polarization\sigma','fontsize',26,'fontweight','bol;

xlabel('Scattering angle (degrees)','fontsize',30,'fontweight','bold');
ylabel('Stokes parameters','fontsize',30,'fontweight','bold');
xlim([-5,360]);
ylim([-1.5,1.5]);

h=get(gcf,'children')
get(h)
set(h,'fontsize',24,'fontweight','bold','box','off','linewidth',2.5)
legend('So','S1','S2','S3','location','EastOutside');

figure(2);
paso = 1:30:1024;
plot(Gr(paso),Sout0p(paso),'.-k',Gr(paso),Sout1p(paso),'-ob',Gr(paso),Sout2p(paso),'-
g*',Gr(paso),Sout3p(paso),'-rv','linewidth',1.4)
hold on
plot(Gr(1:1024),A(1:1024),':k','linewidth',0.5)
hold off

title('Conicalincidence.Polarization\pi','fontsize',26,'fontweight','bold');
xlabel('Scattering angle (degrees)','fontsize',30,'fontweight','bold');
ylabel('Stokes parameters','fontsize',30,'fontweight','bold');
```

```
xlim([-5,360]);
ylim([-1.5,1.5]);

h=get(gcf,'children')
get(h)
set(h,'fontsize',24,'fontweight','bold','box','off','linewidth',2.5)
legend('So','S1','S2','S3','location','EastOutside');

figure(3);
plot(Gr,powerp,'r',Gr,powers,'b')

title('Power','fontsize',12,'fontweight','light');
xlabel('Degrees','fontsize',12,'fontweight','light');
ylabel('Intensity','fontsize',12,'fontweight','light');
xlim([0,370]);

h=get(gcf,'children')
get(h)
set(h,'fontsize',10,'fontweight','light','box','off')
legend('P','S');

%%%%%%%%%%%%%%%%%%%%%%%%%%%%
%%%%%%%%%%%%%%%%%%%%%%%%%%%%
%%%%%%%%%%%%%%%%%%%%%%%%%%%%
%% Data input for the X and Y polarization states

Sx = csvread('x.csv',24,0);
tx = Sx(1:1024,1);
powerx = Sx(1:1024,10);
```

```
Sy = csvread('y.csv',24,0);
ty = Sy(1:1024,1);
powery = Sy(1:1024,10);

% Data input for the X polarization state

DoP = Sx(1:1024,9);
Sout0x = ones(1024,1);
Sout1x = Sx(1:1024,2);
Sout2x = Sx(1:1024,3);
Sout3x = Sx(1:1024,4);

% Data input for the Y polarization state

DoP = Sy(1:1024,9);
Sout0y = ones(1024,1);
Sout1y = Ss(1:1024,2);
Sout2y = Ss(1:1024,3);
Sout3y = Ss(1:1024,4);

% Conversion from dBm to mW

powerx = 10.^(powerx/10);
powery = 10.^(powery/10);
Gr = 0:360/(1024-1):360;
%
Sresx = horzcat(Sout0x,Sout1x,Sout2x,Sout3x);
Sresy = horzcat(Sout0y,Sout1y,Sout2y,Sout3y);

% Plotting
```

```
figure(2);
plot(Gr,Sout0x,'r',Gr,Sout1x,'r',Gr,Sout2x,'r',Gr,Sout3x,'r')
hold on
plot(Gr,Sout0y,'y',Gr,Sout1y,'y',Gr,Sout2y,'y',Gr,Sout3y,'y')
hold off
title('Polarizations X and Y','fontsize',14,'fontweight','bold');
xlabel('Degrees','fontsize',14,'fontweight','bold');
ylabel('Stokes','fontsize',14,'fontweight','bold');
xlim([0,360]);

h=get(gcf,'children')
get(h)
set(h,'fontsize',14,'fontweight','bold','box','off')
legend('X','Y');

%%%%%%%%%%%%%%%%%%%%%%%%%%%%%%
%%%%%%%%%%%%%%%%%%%%%%%%%%%%%%
%%%%%%%%%%%%%%%%%%%%%%%%%%%%%%
%% Data input for the r and l polarization states

Sr = csvread('r.csv',24,0);
tr = Sr(1:1024,1);
powerr = Sr(1:1024,10);

Sl = csvread('l.csv',24,0);
tl = Sl(1:1024,1);
powerl = Sl(1:1024,10);

% Data input for the r polarization state
```

```
DoP = Sr(1:1024,9);
Sout0r = ones(1024,1);
Sout1r = Sr(1:1024,2);
Sout2r = Sr(1:1024,3);
Sout3r = Sr(1:1024,4);

% Data input for the l polarization state

DoP = Sl(1:1024,9);
Sout0l = ones(1024,1);
Sout1l = Sl(1:1024,2);
Sout2l = Sl(1:1024,3);
Sout3l = Sl(1:1024,4);

% Conversion from dBm to mW

powerr = 10.^(powerr/10);
powerl = 10.^(powerl/10);
Gr = 0:360/(1024-1):360;
%
Sresr = horzcat(Sout0r,Sout1r,Sout2r,Sout3r);
Sresl = horzcat(Sout0l,Sout1l,Sout2l,Sout3l);

% Plotting

figure(3);
plot(Gr,Sout0r,'r',Gr,Sout1r,'r',Gr,Sout2r,'r',Gr,Sout3r,'r')
hold on
plot(Gr,Sout0l,'y',Gr,Sout1l,'y',Gr,Sout2l,'y',Gr,Sout3l,'y')
```

```
hold off
title('Polarizations R and L','fontsize',14,'fontweight','bold');
xlabel('Degrees','fontsize',14,'fontweight','bold');
ylabel('Stokes','fontsize',14,'fontweight','bold');
xlim([0,360]);

h=get(gcf,'children')
get(h)
set(h,'fontsize',14,'fontweight','bold','box','off')
legend('R','L');
break
```

Appendix B

In this section we are going to describe the corresponding programs developed in MatLab for the presentation and analysis of the results presented in the previous sections and chapters. The representation of the Stokes parameters that were obtained around to 360º from the scattered light by the metallic thin cylinder, these data were represented by a the Poincaré sphere, where it is possible to observe that the resultant polarizations have a specific behavior like of a retarder wave plate resolved angularly. The optical paths presented in the spheres are the polarimetric results from the cylinder in all of the round trip measured with the PSA.

```
close all
clear all
clc

% In this program can generate the POINCARE SPHERE, the data base in
% this program works with the data generated by a PSA Thorlabs
% polarimeter, calling the data base where the vectors of Stokes were found.

%
% Input data, the results measured by the PSA

Sp = csvread('pplana2.csv',24,0);
Ss = csvread('splana2.csv',24,0);
Sx = csvread('xplana2.csv',24,0);
Sy = csvread('yplana2.csv',24,0);
Sr = csvread('rplana2.csv',24,0);
Sl = csvread('lplana2.csv',24,0);

%%%%
```

```
% Extract data from file for the P Polarization
%%%%

Sout0p = ones(1024,1); % Out Stokes Vector S0
Sout1p = Sp(1:1024,2); % Out Stokes vector S1
Sout2p = Sp(1:1024,3); % Out Sotkes vector S2
Sout3p = Sp(1:1024,4); % Out Stokes vector S3

% The data are separated with the objective to describe the two forms of
% the scattering of the light around of the 360º

Sout0p0 = ones(1024,1); % Out Stokes Vector S0
Sout1p1 = Sp(513:1024,2); % Out Stokes vector S1
Sout2p2 = Sp(513:1024,3); % Out Sotkes vector S2
Sout3p3 = Sp(513:1024,4); % Out Stokes vector S3

%%%%
% Extract data from file for the S Polarization
%%%%

Sout0s = ones(1024,1); % Out Stokes Vector S0
Sout1s = Ss(1:512,2); % Out Stokes vector S1
Sout2s = Ss(1:512,3); % Out Sotkes vector S2
Sout3s = Ss(1:512,4); % Out Stokes vector S3

% The data are separated with the objective to describe the two ways of
% the scattering of the light around of the 360º

Sout0s0 = ones(1024,1); % Out Stokes Vector S0
Sout1s1 = Ss(513:1024,2); % Out Stokes vector S1
```

```
Sout2s2 = Ss(513:1024,3); % Out Sotkes vector S2
Sout3s3 = Ss(513:1024,4); % Out Stokes vector S3

%%%%
% Extract data from file for the X Polarization
%%%%

Sout0x = ones(1024,1); % Out Stokes Vector S0
Sout1x = Sx(1:512,2); % Out Stokes vector S1
Sout2x = Sx(1:512,3); % Out Sotkes vector S2
Sout3x = Sx(1:512,4); % Out Stokes vector S3

% The data are separated with the objective to describe the two ways of
% the scattering of the light around of the 360º

Sout0x0 = ones(1024,1); % Out Stokes Vector S0
Sout1x1 = Sx(513:1024,2); % Out Stokes vector S1
Sout2x2 = Sx(513:1024,3); % Out Sotkes vector S2
Sout3x3 = Sx(513:1024,4); % Out Stokes vector S3

%%%%
% Extract data from file for the Y Polarization
%%%%

Sout0y = ones(1024,1); % Out Stokes Vector S0
Sout1y = Sy(1:512,2); % Out Stokes vector S1
Sout2y = Sy(1:512,3); % Out Sotkes vector S2
Sout3y = Sy(1:512,4); % Out Stokes vector S3

% The data are separated with the objective to describe the two ways of
```

```
% the scattering of the light around of the 360º

Sout0y0 = ones(1024,1); % Out Stokes Vector S0
Sout1y1 = Sy(513:1024,2); % Out Stokes vector S1
Sout2y2 = Sy(513:1024,3); % Out Sotkes vector S2
Sout3y3 = Sy(513:1024,4); % Out Stokes vector S3

%%%%
% Extract data from file for the r Polarization
%%%%

Sout0r = ones(1024,1); % Out Stokes Vector S0
Sout1r = Sr(1:512,2); % Out Stokes vector S1
Sout2r = Sr(1:512,3); % Out Sotkes vector S2
Sout3r = Sr(1:512,4); % Out Stokes vector S3

% The data are separated with the objective to describe the two ways of
% the scattering of the light around of the 360º

Sout0r0 = ones(1024,1); % Out Stokes Vector S0
Sout1r1 = Sr(513:1024,2); % Out Stokes vector S1
Sout2r2 = Sr(513:1024,3); % Out Sotkes vector S2
Sout3r3 = Sr(513:1024,4); % Out Stokes vector S3
%%%%
% Extract data from file for the l Polarization
%%%%

Sout0l = ones(1024,1); % Out Stokes Vector S0
Sout1l = Sl(1:512,2); % Out Stokes vector S1
Sout2l = Sl(1:512,3); % Out Sotkes vector S2
```

```
Sout3l = Sl(1:512,4); % Out Stokes vector S3

% The data are separated with the objective to describe the two ways of
% the scattering of the light around of the 360º

Sout0l0 = ones(1024,1); % Out Stokes Vector S0
Sout1l1 = Sl(513:1024,2); % Out Stokes vector S1
Sout2l2 = Sl(513:1024,3); % Out Sotkes vector S2
Sout3l3 = Sl(513:1024,4); % Out Stokes vector S3

% Stokes vectors transformation to Cartesian system x, y, z in a simple
% manner:

x = Sout1x;
y = Sout2x;
z = Sout3x;
x1 = Sout1x1;
y1 = Sout2x2;
z1 = Sout3x3;

%%
% plot data

figure('Position',[183 70 500 600]);

[X,Y,Z] = sphere(20);
X = X;
Y = Y;
Z = Z;
Hs = mesh(X,Y,Z,'facecolor','w','edgecolor',[0.5 0.5 0.5]);  % set grid facecolor to white
```

```
caxis([1.0 1.01]);  % set grid to appear like all one color
alpha(0.30);  % set opacity of sphere to 70%
axis equal;  % make the three axes equal so the ellipsoid looks like a sphere
set(gcf,'Renderer','opengl');
hold on;

Hx = plot3([-1.5 1.5], [0 0], [0 0],'k-');
set(Hx,'linewidth',2,'linestyle','-','color','k');
ht_x = text(1.75,0,0,'+S_1','fontweight','bold','fontsize',20,'fontname','arial','linewidth',2.5);
Hy = plot3([0 0], [-1.5 1.5], [0 0],'k-');
set(Hy,'linewidth',2,'linestyle','-','color','k');
ht_y = text(0.1,1.6,0,'+S_2','fontweight','bold','fontsize',20,'fontname','arial','linewidth',2.5);
Hz = plot3([0 0], [0 0], [-1.5 1.5],'k-');
set(Hz,'linewidth',2,'linestyle','-','color','k');
ht_z = text(-0.05,0,1.35,'+S_3','fontweight','bold','fontsize',20,'fontname','arial','linewidth',2.5);

% Draw a bold circle about the equator (2*epsilon = 0)

x_e = (-1:.01:1);
for i = 1:length(x_e)
z_e(i) = 0;
y_e_p(i) = +sqrt(1 - x_e(i)^2);
y_e_n(i) = -sqrt(1 - x_e(i)^2);
end
He = plot3(x_e,y_e_p,z_e,'k-',x_e,y_e_n,z_e,'k-');
set(He,'linewidth',2,'color','k');

% Draw a bold circle about the prime meridian (2*theta = 0, 180)

y_pm = (-1:.01:1);
```

```
for i = 1:length(x_e)
x_pm(i) = 0;
z_pm_p(i) = +sqrt(1 - y_pm(i)^2);
z_pm_n(i) = -sqrt(1 - y_pm(i)^2);
end
Hpm = plot3(x_pm,y_pm,z_pm_p,'k-',x_pm,y_pm,z_pm_n,'k-');
set(Hpm,'linewidth',2,'color','k');

%Now plot the polarimetry data


paso = 1:4:512;
H = plot3(x(paso),y(paso),z(paso),'r<');
set(gca,'fontweight','bold','fontsize',20,'fontname','arial');
set(H,'markersize',6,'markeredgecolor','r','markerfacecolor','r','color','r','linewidth',1.4);

hold on
H2 = plot3(x1(paso),y1(paso),z1(paso),'y.');
set(gca,'fontweight','bold','fontsize',20,'fontname','arial');
set(H2,'markersize',15,'markeredgecolor','y','markerfacecolor','y','color','y','linewidth',0.1);
hold off
title('b)','fontweight','bold','fontsize',30,'fontname','arial')
view(135,20);  % change the view angle
```

Appendix C

In this section we are going to describe the corresponding programs developed in MatLab for the presentation and analysis of the results presented in the previous sections and chapters. The representation of the behavior of the cylinder as a retarder wave plate resolved angularly.

```
close all
clear all
clc

% Datos de Entrada Polarizacion +45
Sx = csvread('xplana2.csv',24,0);
% Datos de Entrada Polarizacion -45
Sy = csvread('yplana2.csv',24,0);
% Datos de Entrada Polarizacion r
Sr = csvread('rplana2.csv',24,0);
% Datos de Entrada Polarizacion l
Sl = csvread('lplana2.csv',24,0);
% Datos de Entrada para cuando icidimos Polarizacion +45

Sout2x = Sx(1:1024,3);
Sout2xx = Sx(1:1024,4);
Sout2y = Sy(1:1024,3);
Sout3r = Sr(1:1024,3);
Sout3rr = Sr(1:1024,4);
Sout3l = Sl(1:1024,3);
Sout3ll = Sl(1:1024,4);

Gr = 0:360/(1024-1):360; % aqui introducimos los grados (eje x)
```

```
thetascatt0x = acos(Sout2x);
thetascattx = (thetascatt0x*180)/pi;
thetascatt0xx = asin(-Sout2xx);
thetascattxx = (thetascatt0xx*180)/pi;

thetascatt0y = acos(-Sout2y);
thetascatty = (thetascatt0y*180)/pi;

thetascatt0r = acos(Sout3r);
thetascattr = (thetascatt0r*180)/pi; % here we add 90 degrees for the dephase

implisit in the generation of r
thetascatt0rr = asin(-Sout3rr)+pi/2;
thetascattrr = (thetascatt0rr*180)/pi; % here we add 90 degrees for the

dephase implisit in the generation of r

thetascatt0l = acos(-Sout3l);
thetascattl = (thetascatt0l*180)/pi;
thetascatt0ll = asin(Sout3ll);
thetascattll = (thetascatt0ll*180)/pi; % here we add 90 degrees for the
dephase implisit in the generation of r

figure(1);
paso = 1:11:1024;
plot(Gr(paso), thetascattx(paso),'-g*',Gr(paso), thetascattrr(paso),'-rv','linewidth',1.4)
%plot(Gr(paso), thetascattr(paso),'linewidth',1.4)
hold on
line('XData', [146.7 146.7], 'YData', [185 0], 'LineStyle', '-','LineWidth', 2, 'Color','k')
hold on
```

```
line('XData', [-5 360], 'YData', [90 90], 'LineStyle', '-','LineWidth', 2, 'Color','k')
hold on
line('XData', [207.5 207.5], 'YData', [185 0], 'LineStyle', '-','LineWidth', 2, 'Color','k')

legend('a)','b)','location','EastOutside');
xlabel('Scattering angle (degrees)','fontsize',30,'fontweight','bold');
ylabel('\delta (degrees)','fontsize',30,'fontweight','bold');
xlim([-5,360]);
ylim([0,185]);
h = get(gcf,'children');
set(h,'fontsize',24,'fontweight','bold','box','off','linewidth',2.5)
```

Appendix D

In this part of the thesis, we are going to describe the rest of the analysis for the ±45º and right and left hand circular polarization states. The experimental setup (**Fig.3.1.2**, Chapter 3) shows the form of how the PSG generate all the homogeneous polarizations and the make them interact with the cylinder. In the next Figures we are going to find the Stokes behavior of this phenomenon around 360º and the optical path described on the Poincaré sphere.

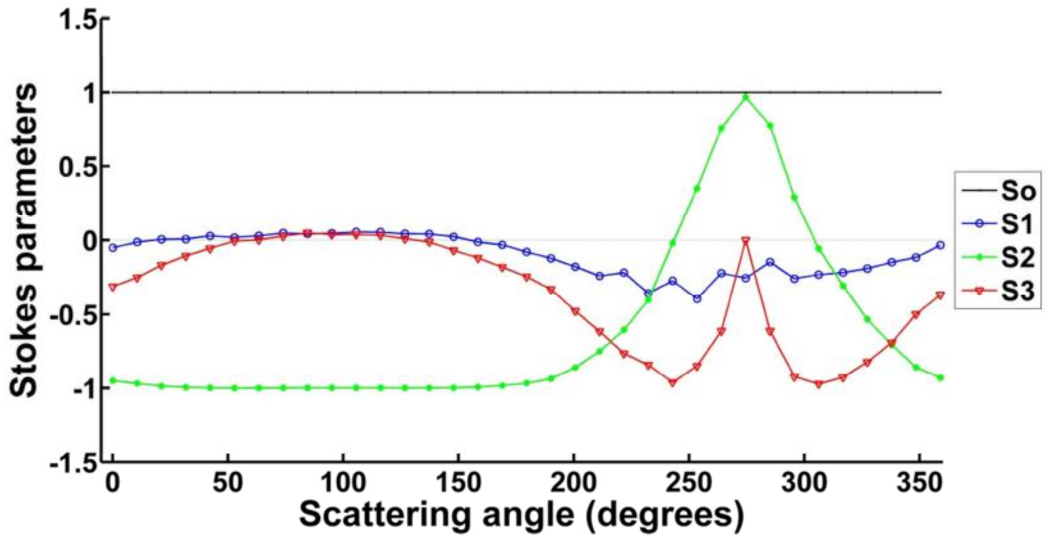

Fig. AD1 Scattered Stokes parameters versus scattering angle when an aluminum cylinder is illuminated by a +45º polarization state θ_0=0 degrees and conical angle φ=4º.

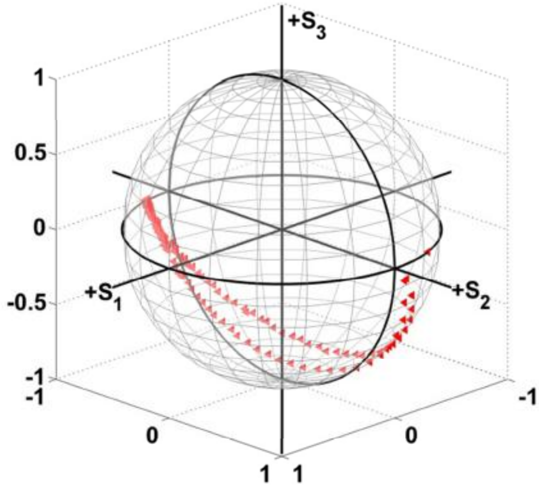

Fig. AD2 Light scattered by the metallic cylinder (aluminum cylinder) when an incident beam interact with a +45º polarization state, θ_0=0º and conical angle φ=4º. The Poincaré sphere shows the polarimetric behavior of the cylinder around the 360º.

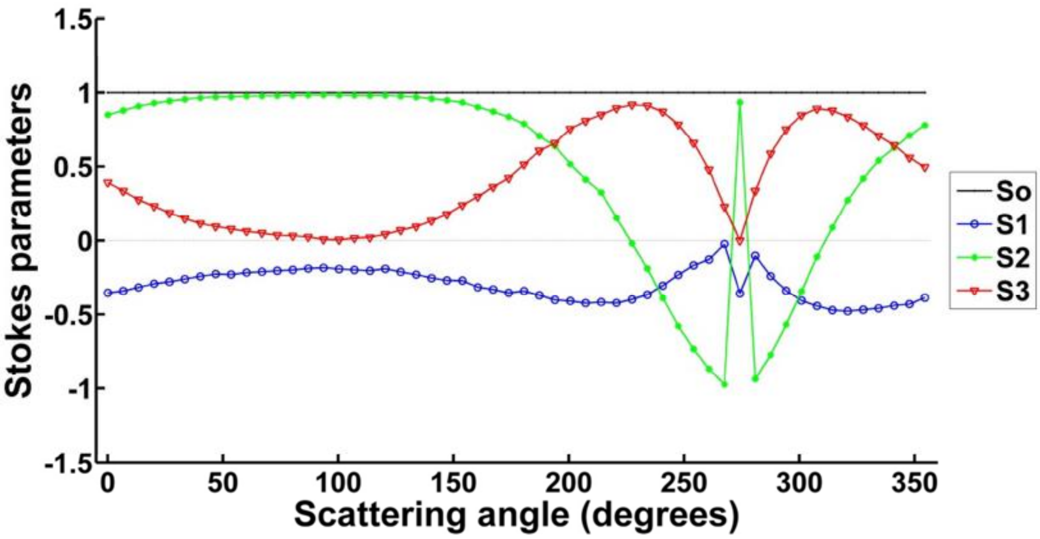

Fig. AD3 Scattered Stokes parameters versus scattering angle when an aluminum cylinder is illuminated by a -45º polarization state θ_0=0 degrees and conical angle φ=4º.

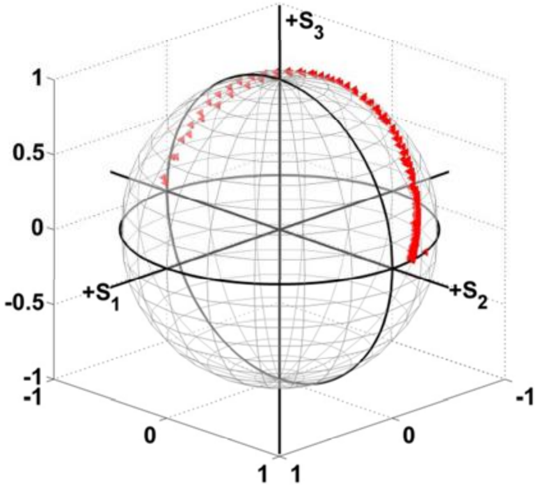

Fig. AD4 Light scattered by the metallic cylinder (aluminum cylinder) when an incident beam interact with a -45º polarization state, θ_0=0º and conical angle φ=4º. The Poincaré sphere shows the polarimetric behavior of the cylinder around the 360º.

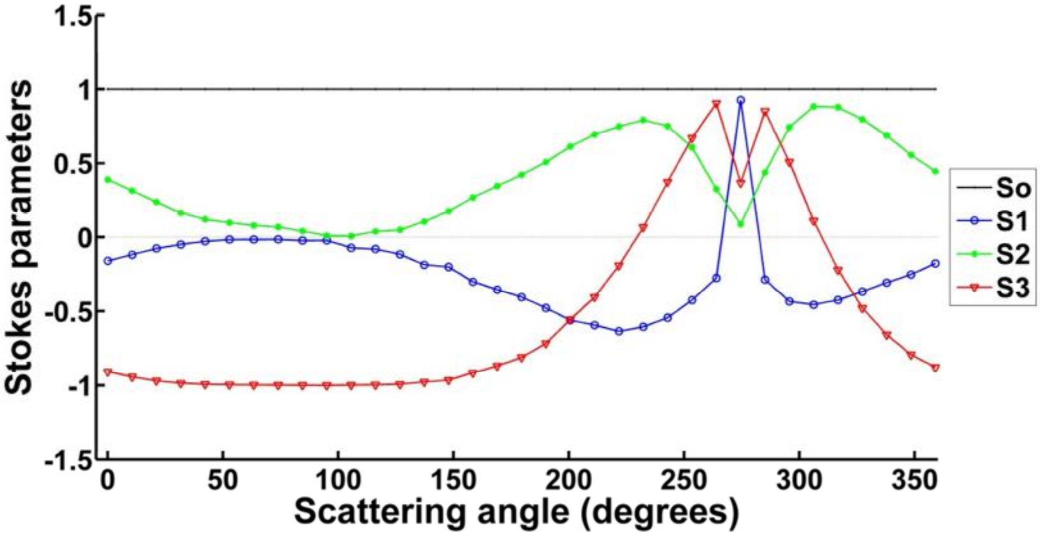

Fig. AD5 Scattered Stokes parameters versus scattering angle when an aluminum cylinder is illuminated by a circular right hand polarization state (r) θ_0=0 degrees and conical angle φ=4º.

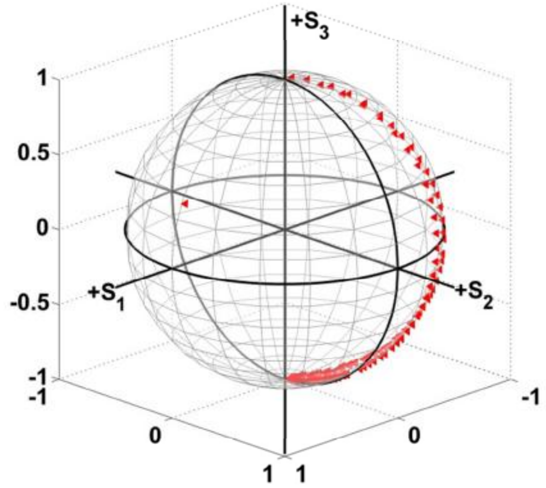

Fig. AD6 Light scattered by the metallic cylinder (aluminum cylinder) when an incident beam interact with a circular right hand polarization state (r), θ_0=0º and conical angle φ=4º. The Poincaré sphere shows the polarimetric behavior of the cylinder around the 360º.

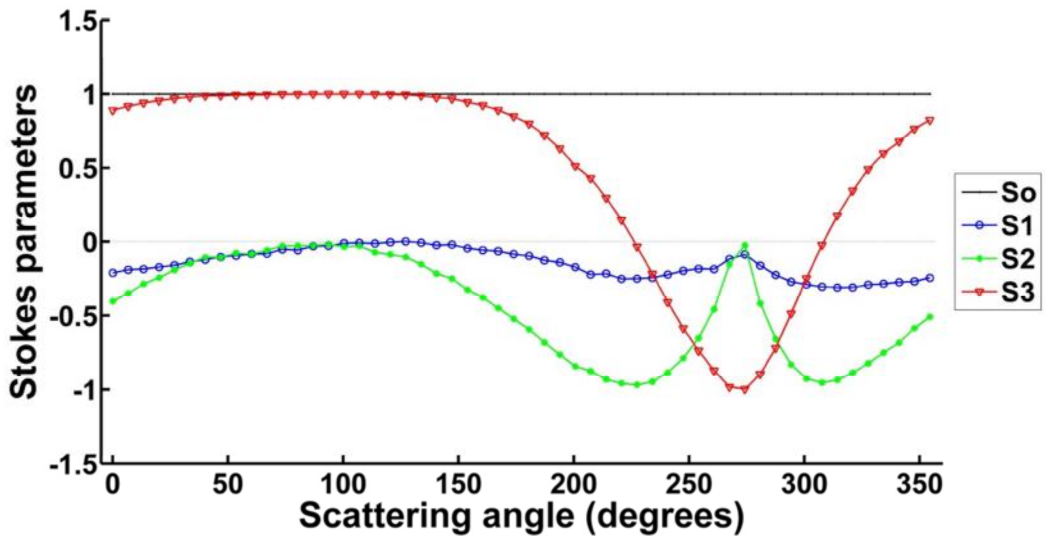

Fig. AD7 Scattered Stokes parameters versus scattering angle when an aluminum cylinder is illuminated by a circular left hand polarization state (l) θ_0=0 degrees and conical angle φ=4º.

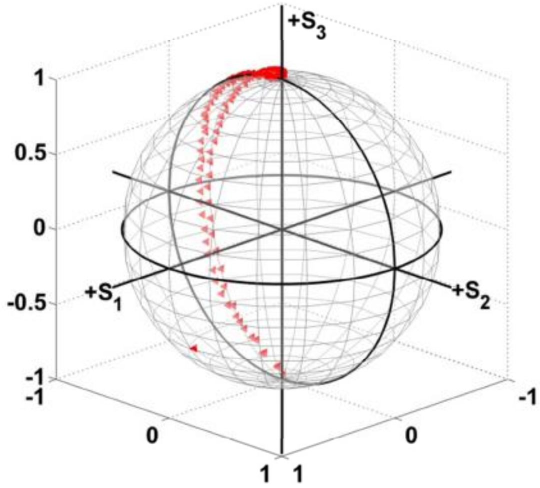

Fig. AD8 Light scattered by the metallic cylinder (aluminum cylinder) when an incident beam interact with a circular left hand polarization state (l), θ_0=0º and conical angle φ=4º. The Poincaré sphere shows the polarimetric behavior of the cylinder around the 360º.

Appendix E

The images of the fiber recovered with aluminum and the nickel (guitar string) were taken with a Zeiss LSM 710 NLO (Multiphoton Microscopy) [60].

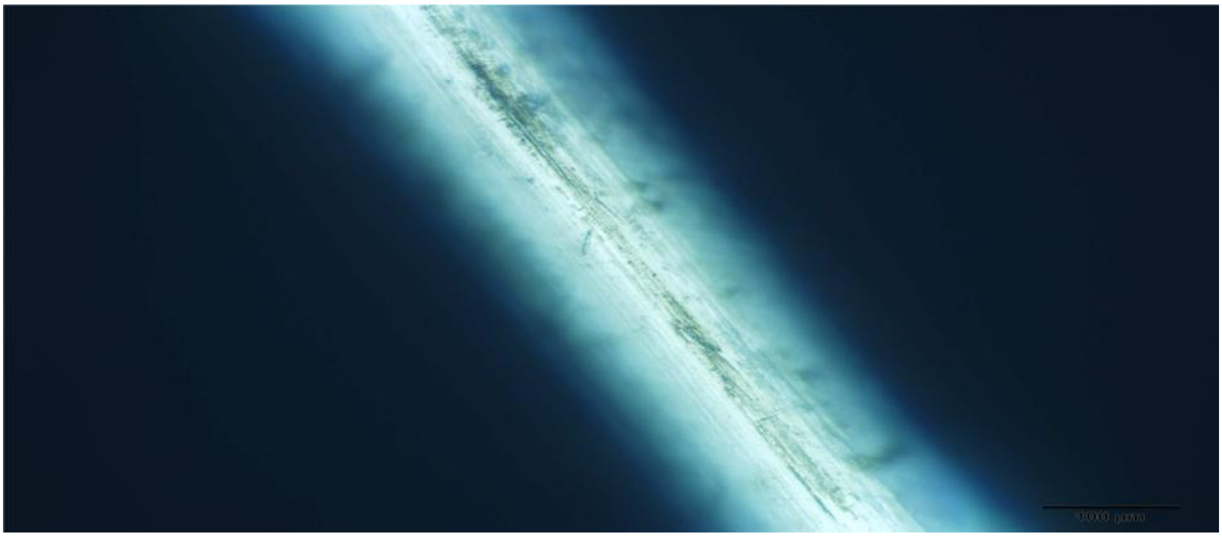

Image 1. Nickel cylinder (string guitar), diameter of 254 µm.

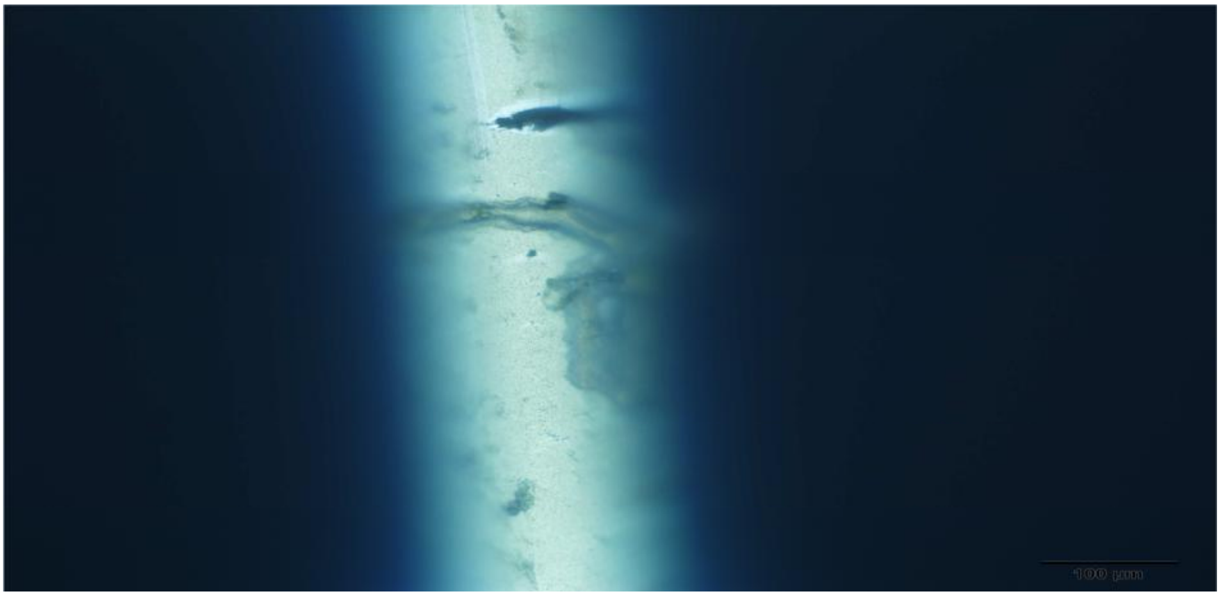

Image 2. Optical fiber covered with a uniformly distributed aluminum thin film, diameter of 232 µm.